AD-A051 450 FLORIDA UNIV GAINESVILLE DEPT OF ENGINEERING SCIENCES F/G 10/2
TWO-PHASE HARTMANN FLOWS IN THE MHD GENERATOR CONFIGURATION.(U)
FEB 78 R E ELKINS, U H KURZWEG N00014-76-C-0410
UNCLASSIFIED NL

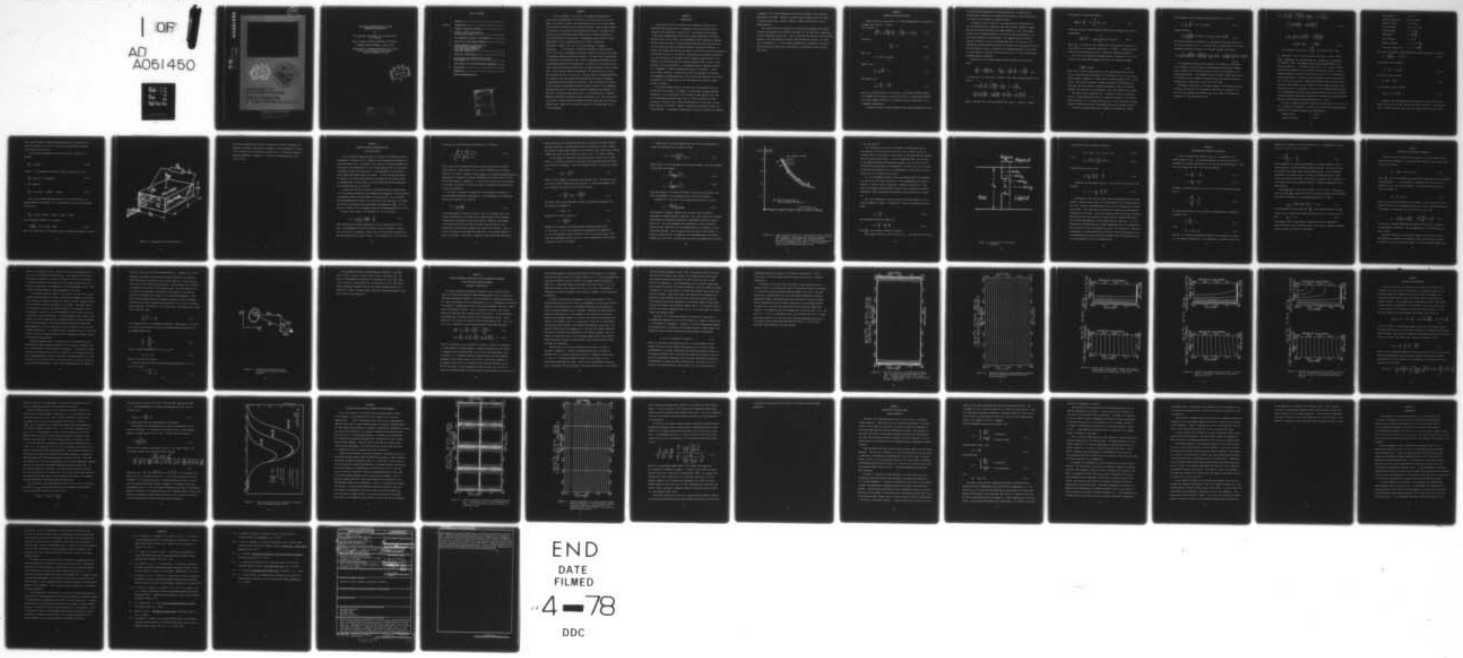

END
DATE FILMED
4-78
DDC

DEPARTMENT OF ENGINEERING SCIENCES

College of Engineering
University of Florida Gainesville, FL 32611

TWO PHASE HARTMANN FLOWS IN THE MHD GENERATOR CONFIGURATION

by

U.H. Kurzweg, R.E. Elkins, T.A. Trovillion and
E.R. Lindgren

Dept. of Engin. Sciences, University of Florida

TECHNICAL REPORT NR 01-001, January 1978

Annual Report on Research Sponsored by U.S. Navy,
Office of Naval Research, Power Branch
Contract No N00014-76-C-0410

TABLE OF CONTENT

ABSTRACT

A full treatment of the flow in a two-phase Faraday generator must include consideration of the inertial and viscous forces in the gas phase, the inertial, viscous, and ponderomotive forces in the liquid phase, and the surface forces at the gas/liquid interfaces. Since the mass density and viscosity of the liquid are much greater than those of the gas, consideration of the liquid phase alone should lead to a good description of force distribution in the generator. Averaging the motion over the liquid phase gives us a set of equations which are similar to equations describing a steady flow of a fluid with spatially variable properties. In this report, we discuss solutions of these equations, first in the limit of negligible inertia and viscosity, and then in the limit of negligible inertia and non-zero viscosity. The first case, corresponding to conditions in the generator core, leads to expressions describing the averaged pressure gradient in the generator. In this vein, we discuss also the cross stream pinch pressure gradient and its possible effects on the two phase flow. The second case leads to expressions of the motion which are valid near the walls as well as in the core. The wall region in Faraday generators is a region of very large shear and ponderomotive forces, and is important in determining efficient generator operation. This is especially noticed in finite difference calculations carried out under a variety of electrodynamic conditions and also in a successful analytical boundary layer approach. On this base a section has been devoted also to the possibilities of improved generator efficiency by subpartitioning the generator duct. The last section of the report concerns similitude between two-phase generators and two-phase gravity flows. There are two velocity scales in the systems which must be scaled separately.

CHAPTER 1

INTRODUCTION

During the last two years analytical and numerical studies on two-phase MHD flows through ducts of rectangular cross sections have been in progress at the University of Florida [1]. This program has been aimed to gain better understanding of the flow processes occurring in two-phase MHD flows and to aid in some of the experimental efforts underway at Argonne National Laboratory (ANL) on liquid metal-gas MHD power generation [2,3,4,5]. Our objectives have been to calculate expected cross-stream variations in velocity and current distribution for flows of specified cross-stream variation in void fraction and also to try better to understand the mechanisms responsible for slip occurring as the two-phase mixture expands through the duct in the presence of an externally applied transverse magnetic field. Both of these problems are of major interest in determining whether a proposed upscaling to a 30 megawatt or larger two-phase MHD generator is feasible. If they can be made to function, such MHD devices have the advantage over standard high temperature gas MHD generators in that their power densities are an order of magnitude or so higher and that the high temperature electrode erosion problem is reduced.

This report presents some of the results we have obtained during the second year of our studies. In Chapter 2, we show that averaged equations of motion for the liquid phase of the two-phase Faraday generator are similar to equations describing steady flow of a fluid of spatially varying properties. Chapters 3 and 4 discuss these equations in the limit of negligible viscosity and inertia. Chapter 5 addresses the problem of phase slip in the generator. The physical consequences of non-zero viscosity are examined

in Chapter 6 by a finite difference solution and in Chapter 7 by an approximate analytic solution. Chapter 8 discusses channel subpartioning as a means of reducing phase slip. Finally, Chapter 9 examines similitude in the two phase generator.

The research has been conducted by co-principal investigators Drs. Elkins, Kurzweg, and Lindgren and by research associate, Mr. Tom Trovillion, completing his Ph.D. dissertion in this area. Part of this work was reported at the thirtieth meeting of the Fluid Mechanics Division, American Physical Society, Nov 21-23, 1977 in Bethlehem, Pa. A more complete presentation is planned for the Second Bat-Sheva Seminar on MHD Flows and Turbulence at Beer-Sheva, Israel on March 28-31,1978.

CHAPTER 2

AVERAGED EQUATIONS OF MOTION

Motion within the liquid phase of a two phase MHD generator is described by Hughes and Young [6]. We have

force balance:

$$\rho\left(\frac{\partial u_i}{\partial t} + u_j \frac{\partial u_i}{\partial x_j}\right) + \frac{\partial P}{\partial x_i} = \mu \frac{\partial^2 u_i}{\partial x_j \partial x_j} + e_{ijk} J_j B_k ; \qquad (2.1)$$

continuity:

$$\frac{\partial u_i}{\partial x_i} = 0 ; \qquad (2.2)$$

Ohm's law:

$$J_i = \sigma(E_i + e_{ijk} u_j B_k) ; \qquad (2.3)$$

Ampére's law:

$$\frac{1}{\mu_e} e_{ijk} \frac{\partial B_k}{\partial x_j} = J_i ; \qquad (2.4)$$

and Farady's law:

$$e_{ijk} \frac{\partial E_k}{\partial x_j} = - \frac{\partial B_i}{\partial t} ; \qquad (2.5)$$

where u_i is liquid velocity, P is pressure, J_i is electric current density, B_i is magnetic flux density, E_i is electric field, ρ is liquid mass density, μ is liquid dynamic viscosity, σ is liquid electrical conductivity, and μ_e is magnetic permeability.

A complete solution of these equations would require consideration also

of equations describing motion of the gas phase and of equations describing stress conditions at the gas/liquid interfaces. That problem is far too complex to be attacked in a general fashion.

An observer fixed in space in a two phase generator should expect to see fluctuating physical conditions, both from alternate passage of phases and from flow variations within each phase separately. Yet certain quantities, such as pressure gradient, void fraction, and current density, are most easily measured as time averages. This suggests that we attempt to describe the motion in terms of averaged quantities. We find that, once assumptions are made about distribution of stresses and configuration of electric and magnetic fields, the Eulerian time averaged equations of motion take on forms similar to equations describing the motion of a fluid with spatially dependent material properties.

Elimination of the current density between equations (2.1) and (2.3) gives

$$\rho\left(\frac{\partial u_i}{\partial t} + u_j\frac{\partial u_i}{\partial x_j}\right) + \frac{\partial P}{\partial x_i} = \mu\frac{\partial^2 u_i}{\partial x_j \partial x_j} + \frac{1}{\mu_e}\left(B_j\frac{\partial B_i}{\partial x_j} - B_j\frac{\partial B_j}{\partial x_i}\right) \qquad (2.6)$$

If dissipation in the gas phase is neglible, then time averaging equation (2.6) gives us

$$\rho(1-\alpha)\left(\bar{u}_j\frac{\partial \bar{u}_i}{\partial x_j} + \overline{\bar{u}'_j\frac{\partial u'_i}{\partial x_i}}\right) + \left\langle\frac{\partial P}{\partial x_i}\right\rangle = \mu(1-\alpha)\frac{\partial^2 \bar{u}_i}{\partial x_j \partial x_j} +$$

$$\frac{1}{\mu_e}\left(\left\langle B_j\right\rangle\left\langle\frac{\partial B_i}{\partial x_j}\right\rangle - \left\langle B_j\right\rangle\left\langle\frac{\partial B_j}{\partial x_i}\right\rangle + \left\langle B'_j\frac{\partial B'_i}{\partial x_j}\right\rangle - \left\langle B'_j\frac{\partial B'_j}{\partial x_i}\right\rangle\right) \qquad (2.7)$$

where α indicates the local time average void fraction. Brackets indicate

the complete time averaging operator

$$\left\langle \mathcal{F}(x_i, t) \right\rangle \equiv \frac{1}{T} \int_0^T \mathcal{F}(x_i, t)dt \tag{2.8}$$

Overscores indicate a time averaging operator which operates only over the liquid phase

$$\overline{\mathcal{F}(x_i, t)} \equiv \frac{1}{T(1-\alpha)} \int_0^T \mathcal{F}(x_i,t)\ \delta(x_i,t)dt \tag{2.9}$$

where $\delta(x_i, t)$ is equal to unity whenever the liquid phase is present at x_i and is equal to zero otherwise. (Note that $\alpha = 1 - \left\langle \delta \right\rangle$). Primed quantities indicate time fluctuating portions of respective unprimed quantities.

The use of two different averaging operators in equation (2.7) is justified by the relationship between the bracket and overscore averages

$$\left\langle \beta \mathcal{F} \right\rangle = \beta(1-\alpha)\overline{\mathcal{F}} \tag{2.10}$$

where β is a constant scalar property of the liquid phase which is equal to zero in the gas phase and where $\mathcal{F}$ is a functional of u_i, B_i, E_i, and J_i. From a physical standpoint, it makes sense to express equation (2.7) in this fashion. The bracket averages of pressure gradient and flux density are those most easily perceived by external measurements, while the overscore average of the velocity is more relevant to the actual motion of the liquid.

The inertia term in equation (2.7) is similar in form to the inertia term for a fluid whose mass density is a function of position. The viscous term in equation (2.7) is simpler than that for a fluid of spatially varying viscosity, where the viscosity would appear within the divergence operator.

To obtain an equation describing transport of averaged flux density,

first eliminate current density between equations (2.3) and (2.4):

$$\frac{1}{\mu_e} e_{ijk} \frac{\partial B_k}{\partial x_j} = \sigma(E_i + e_{ijk} u_j B_k) \tag{2.11}$$

Average as before

$$\frac{1}{\mu_e} e_{ijk} \left\langle \frac{\partial B_k}{\partial x_j} \right\rangle = \sigma(1-\alpha)\bar{E}_i + \sigma(1-\alpha) e_{ijk} (\bar{u}_j \bar{B}_k + \overline{u'_j B'_k}) \tag{2.12}$$

The overscore average of Faraday's law eliminates the electric field from the curl of equation (2.12). In the same step, we assume that the overscore averaged flux density is equal to the bracket averaged flux density

$$\frac{1}{\mu_e} \frac{\partial}{\partial x_j} \left(\frac{1}{\sigma(1-\alpha)} \left(\left\langle \frac{\partial B_j}{\partial x_i} \right\rangle - \left\langle \frac{\partial B_i}{\partial x_j} \right\rangle \right) \right) = \frac{\partial}{\partial x_j} \left(\bar{u}_i \langle B_j \rangle - \bar{u}_j \langle B_i \rangle \right) + \frac{\partial}{\partial x_j} \left(\overline{u'_i B'_j} - \overline{u'_j B'_i} \right) \tag{2.13}$$

The assumption concerning the averages of flux density is equivalent to an assumption of good electrical connectedness between liquid elements since it implies that the induced electric field is not balanced by local charge distributions. This assumption may be invalid at large void fractions. In a droplet flow, for example, the space charge will exactly balance the induced electric field over at least part of the flow.

Experiments with flows in the Faraday generator configuration reported by Harris [7] show that the flux density correlations in equations (2.7) and (2.13) are typically much smaller than other terms in the respective equations. We drop those terms to get

$$\rho(1-\alpha)\left(\bar{u}_j \frac{\partial \bar{u}_i}{\partial x_j} + \overline{u'_j \frac{\partial u'_i}{\partial x_j}}\right) + \left\langle \frac{\partial P}{\partial x_i} \right\rangle = \mu(1-\alpha) \frac{\partial^2 \bar{u}_i}{\partial x_j \partial x_j} +$$

$$\frac{1}{\mu_e}\left(\left\langle B_j \right\rangle \left\langle \frac{\partial B_i}{\partial x_j} \right\rangle - \left\langle B_j \right\rangle \left\langle \frac{\partial B_j}{\partial x_i} \right\rangle \right) \tag{2.14}$$

$$\frac{1}{\mu_e} \frac{\partial}{\partial x_j}\left(\frac{1}{\sigma(1-\alpha)} \left(\left\langle \frac{\partial B_j}{\partial x_i} \right\rangle - \left\langle \frac{\partial B_i}{\partial x_j} \right\rangle \right) \right) =$$

$$\frac{\partial}{\partial x_j}\left(\bar{u}_i \left\langle B_j \right\rangle - \bar{u}_j \left\langle B_i \right\rangle \right) \tag{2.15}$$

The "Reynolds stress" term, $\overline{u'_j \frac{\partial u'_i}{\partial x_j}}$, of equation (2.14) would be significant only for self-preserving turbulence. Since experiments of Branover [8] indicate that such turbulence is suppressed in Hartmann flows, the Reynolds stress may be insignificant in the two-phase generator. Important viscous effects in a large Hartmann number Faraday generator occur very close to the walls (see ref. [6])and probably dominate the inertial effects there (see ref. [7]). Ponderomotive forces seem likewise to dominate inertial effects in the core region (see ref. [7] and also the order of magnitude discussion later in this chapter). We believe that insight into the behavior of the two-phase generator can be gained from a study of equations (2.14) and (2.15) without inertial effects. It is interesting to note that these equations differ only in the viscosity term from equations describing a steady flow of spatially varying properties. They will be discussed in more detail Chapters 6,7, and 8.

An order of magnitude analysis suggests that equations (2.14) and (2.15) can be simplified considerably. The NaK - N_2 device at the Argonne National Laboratory [3] operates typically with the parameters

channel length $\ell = .385$ m

channel half width $a = 10^{-2}$ m

void fraction	$\alpha = 0.5$
applied flux density	$B_2 = 1.2$ Tesla
terminal voltage	$V = 0.8$ volt
load resistance	$R_e = 5 \times 10^{-4}$ ohm
surface tension	$\gamma = 0.12 \frac{N}{m}$
mass density	$\rho = 890 \frac{kg}{m^3}$
liquid velocity	$U = 10 \frac{m}{s}$
dynamic viscosity	$\mu = 5 \times 10^{-4} \frac{kg}{m.s}$
electrical conductivity	$\sigma = 2.7\ 10^6 \frac{mho}{m}$

Away from the boundaries, the ponderomotive stress gradient is, typically,

$$T_p = \frac{V \cdot B_2}{Ra\ell(1-\alpha)} = 10^6 \frac{N}{m^3} \quad ; \tag{2.16}$$

the inertial stress gradient,

$$T_I = \rho \frac{u^2}{\ell} = 1.5.10^5 \frac{N}{m^3} \quad ; \tag{2.17}$$

the viscous stress gradient

$$T_v = \frac{\mu U}{a^2} = 40 \frac{N}{m^3} \quad ; \tag{2.18}$$

the interfacial stress gradient

$$T_s = \frac{\gamma}{a^2} = 1.2.10^3 \frac{N}{m^3} . \tag{2.19}$$

Evidently, the ponderomotive stress should be at least several times larger than any of the other stresses over most of the flow. The above analysis is invalid near the walls, where the length scales are much smaller.

Near a solid boundary, viscous stresses and, perhaps in turbulent flows, inertial stresses are apt to be as large as the ponderomotive stresses (see references [6] and [7]).

In the limit of negligible inertia and viscosity, equation (2.1) becomes

$$\frac{\partial P}{\partial x_i} = e_{ijk} J_j B_k \tag{2.20}$$

Equation (2.3) eliminates the current density from equation (2.20):

$$\frac{\partial P}{\partial x_i} = e_{ijk}\, \sigma(E_j + e_{jmn} U_m B_n) B_k \tag{2.21}$$

or, upon expansion

$$\frac{\partial P}{\partial x_i} = e_{ijk}\, \sigma E_j B_k + \sigma u_k B_k B_i - \sigma u_i B_k B_k \tag{2.22}$$

Let x_1 be the downstream direction and x_2 be the direction of the applied magnetic flux (Figure 2.1). Then equation (2.22) in the downstream direction is,

$$\frac{\partial P}{\partial x_1} = \sigma(-E_3 B_2 + u_2 B_2 B_1 - u_3 B_3 B_1 - u_1 B_2 B_2 - u_1 B_3 B_3)$$

Time averaging of equation (2.23) leads to

$$\left\langle \frac{\partial P}{\partial x_1} \right\rangle = -(1-\alpha)\sigma\, (\bar{E}_3 \bar{B}_2 - \bar{u}_1 \bar{B}_2^2) \tag{2.24}$$

where the correlations of fluctuating terms are neglected and where, as before,

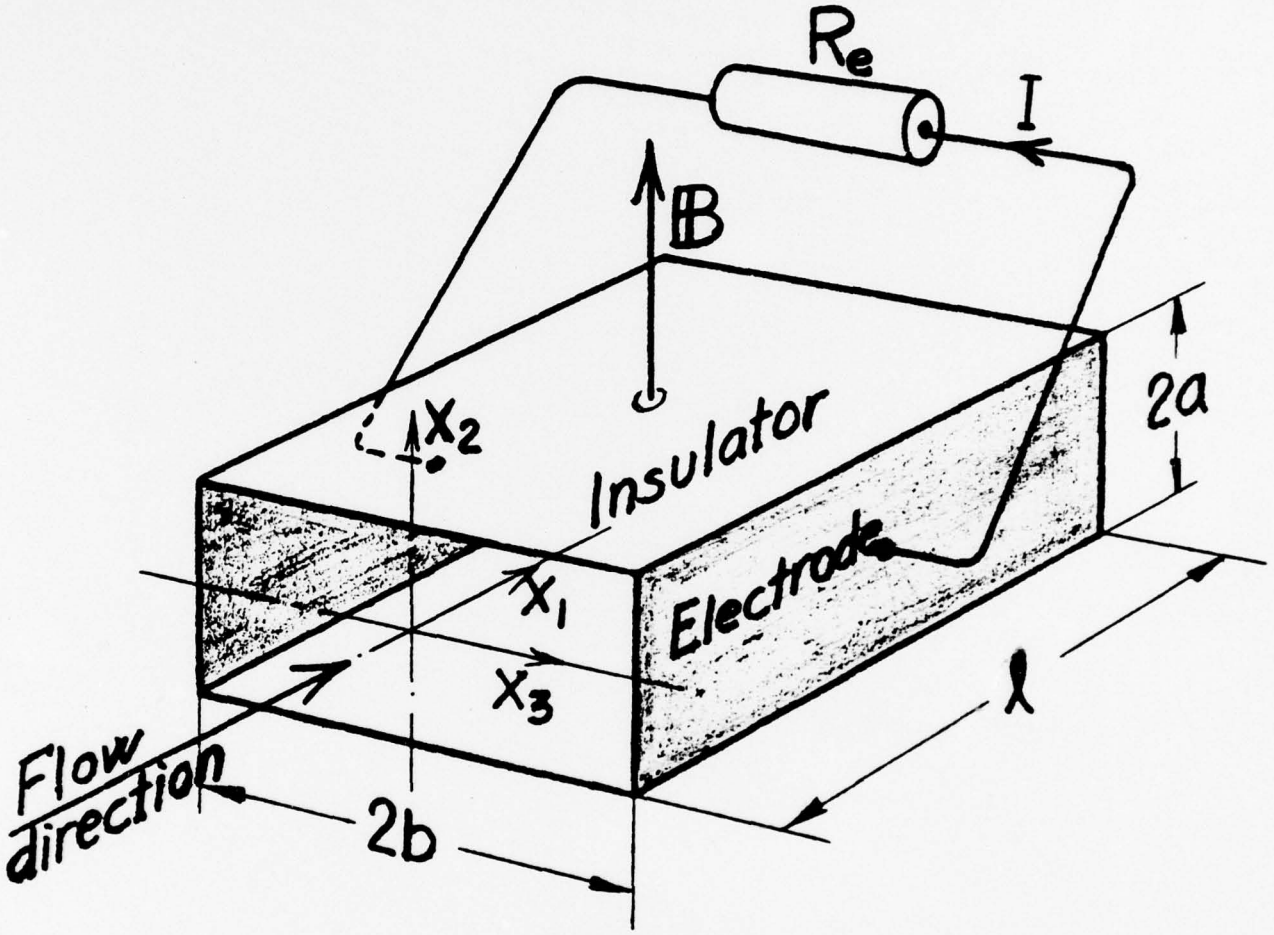

Figure 2.1 Configuration of Faraday generator.

the bracket averages over the electric field and over the flux density are assumed to be equal to the overscore averages. As with equations (2.14) and (2.15), equation (2.24) describes the steady flow of a fluid with spatially varying conductivity. Chapters 3, 4, and 5 will discuss equation (2.24) in more detail.

CHAPTER 3

MASSLESS INVISCID APPROXIMATION FOR THE LIQUID PHASE

A set of specific assumptions about the electric field permits certain developments of equation (2.15), leading to some interesting conclusions concerning two phase flow. In contrast to the case of a classical Hartmann flow, the electric field produced by flow in a finite generator may not be uniform (see Hughes & Young [6]). This is due to the development of a non-uniform space charge distribution within the channel. In the following discussions of equation (2.24) and related equations, we assume that this space charge is insignificant or, which leads to the same thing, that the flow properties do not change along the x_3 direction.

It might be noted that the direct relationship between liquid fraction $(1-\alpha)$ and apparent conductivity also depends on an assumption of good electrical connectedness between liquid elements in the x_3 direction. As α increases, this connectedness will degrade more and more so that equation (2.24), given the velocity distribution, will overestimate the magnitude of $\frac{\partial \bar{P}}{\partial x_1}$. In the limit of a droplet flow, for example, there are no ponderomotive forces at all.

Equation (2.24) leads to an expression for velocity profile

$$\bar{u}_1 = + \frac{1}{\bar{B}^2 \sigma(1-\alpha)} \left\langle \frac{\partial P}{\partial x_1} \right\rangle + \frac{\bar{E}_3}{\bar{B}_2} \tag{3.1}$$

which demonstrates an inverse dependence on local liquid fraction $(1-\alpha)$. Thus, the ponderomotive force will drive the liquid in regions of large α. This can result in an apparent, overall slip of the gas phase even when the gas and liquid are well coupled locally, If we assume that, locally, gas and

liquid move at the same velocity then the slip χ is given by

$$\chi = \frac{\int_S (1-\alpha)\ dS \int \alpha\ \bar{u}_1\ dS}{\int_S \alpha\ dS \int_S (1-\alpha)\bar{u}_1\ dS} \tag{3.2}$$

which is the ratio of mean gas velocity to mean liquid velocity at some cross section S. When equation (3.1) is used to evaluate $\bar{u}_1$ to be used in equation (3.2), then x is equal to unity whenever α is constant everywhere across S. Departures of α from such a constant distribution will always lead to a slip greater than unity in a generator. In view of this, some of the slip reported for the Nak - N_2 device at ANL must be linked to observed cross stream variations in void fraction.

It is also of interest to examine the current density distribution in the same magnetoaerodynamic approximation. Time averaging in the downstream direction of equation (2.1) leads to

$$\bar{J}_3 = -\frac{1}{\bar{B}_2}\left\langle \frac{\partial P}{\partial x_1} \right\rangle \tag{3.3}$$

to the same degree of accuracy as before. This is a statement that, over a given cross section, the average local current density will be constant irrespective of variations in the void fraction. Evidently, the dynamics of the system are such as to adjust the local liquid velocity so as to maintain the current density constant over a given cross section. There is no short circuiting as one might have expected to occur through regions of small void fraction. With this, it seems that phase separation reduces ope-

rating efficiency, not through internal short circuiting, but rather through increased pump work in maintaining the high velocities of the large α regions and through increased ohmic dissipation in regions of high, liquid phase currents (higher than local average current by a factor $(1-\alpha)^{-1}$) of large α regions.

In the absence of significant inertial and viscous forces in the liquid phase, it is possible to derive an expression relating pressure drop and electric field in the generator. The total external current I in that case (Figure 2.1) is

$$I = \frac{V}{R_e} = -\frac{2b\ E_3}{R_e} \tag{3.4}$$

where V is the terminal voltage and R_e the external load. The current I also is the net current flowing across the channel. If the applied magnetic flux B_2 is uniform, then the net force F on the liquid is

$$F = -\frac{2b\ E_3}{R_e}\ B_2 2b = -\frac{4b^2 E_3 B_2}{R_e} \tag{3.5}$$

The force F also can be expressed in terms of the pressure change ΔP over the length of the generator:

$$F = 4ab^2\ \ \Delta P \tag{3.6}$$

Equations (3.5) and (3.6) give us

$$E = -\frac{R_e\ a\ \Delta P}{b\ B_2} \tag{3.7}$$

Equation (3.7) amounts to an energy balance, equating pressure work to Joule work. It can thus be expected to overestimate the magnitude of E_3 in a real generator, since it does not account for viscous losses. Note that the relationship between E_3 and ΔP occurs irrespective of the detailed structure of flow in the channel.

Integration of the time averaged Ohm's law over the entire generator leads to an expression for the electric field:

$$E_3 = -B_2\hat{u}_1 \frac{\sigma(1-\hat{\alpha})}{\frac{b}{R_e aL} + \sigma(1-\hat{\alpha})} \tag{3.8}$$

where $\hat{u}_1$ and $\hat{\alpha}$ are the averages over the entire channel of the time averaged velocity and void fraction:

$$\hat{u} \equiv \frac{\int_{\text{channel}} \bar{u}_1 \, dV}{4\ell ab} \tag{3.9}$$

$$\hat{\alpha} \equiv \frac{\int_{\text{channel}} \alpha \, dV}{4\ell ab} \tag{3.10}$$

Note that equation (3.8) arises from Ohm's law and circuit continuity, and thus is independent of any assumptions about inertia or viscosity.

Equations (3.7) and (3.8) can be equated and solved for ΔP to give

$$\Delta P = \frac{\ell b B_2^2 \, \sigma \hat{u}_1}{b + R_e \sigma \ell a(1-\hat{\alpha})} \tag{3.11}$$

This expression estimates pressure drop from data readily obtained in experiments at Argonne National Laboratory. But, since $\hat{u}_1$ and $\hat{\alpha}$ are obtained from integrals over measured quantities, nonsystematic errors will tend to smooth out. Thus, fair agreement with experiment ΔP can be obtained by measuring inlet conditions only and assuming nearly any reasonable flow distribution downstream. Such a procedure has been used to obtain Figure 3.1, where the liquid velocity is assumed to vary one-dimensionally and linearly between inlet and outlet, and where gas and liquid are assumed to move locally

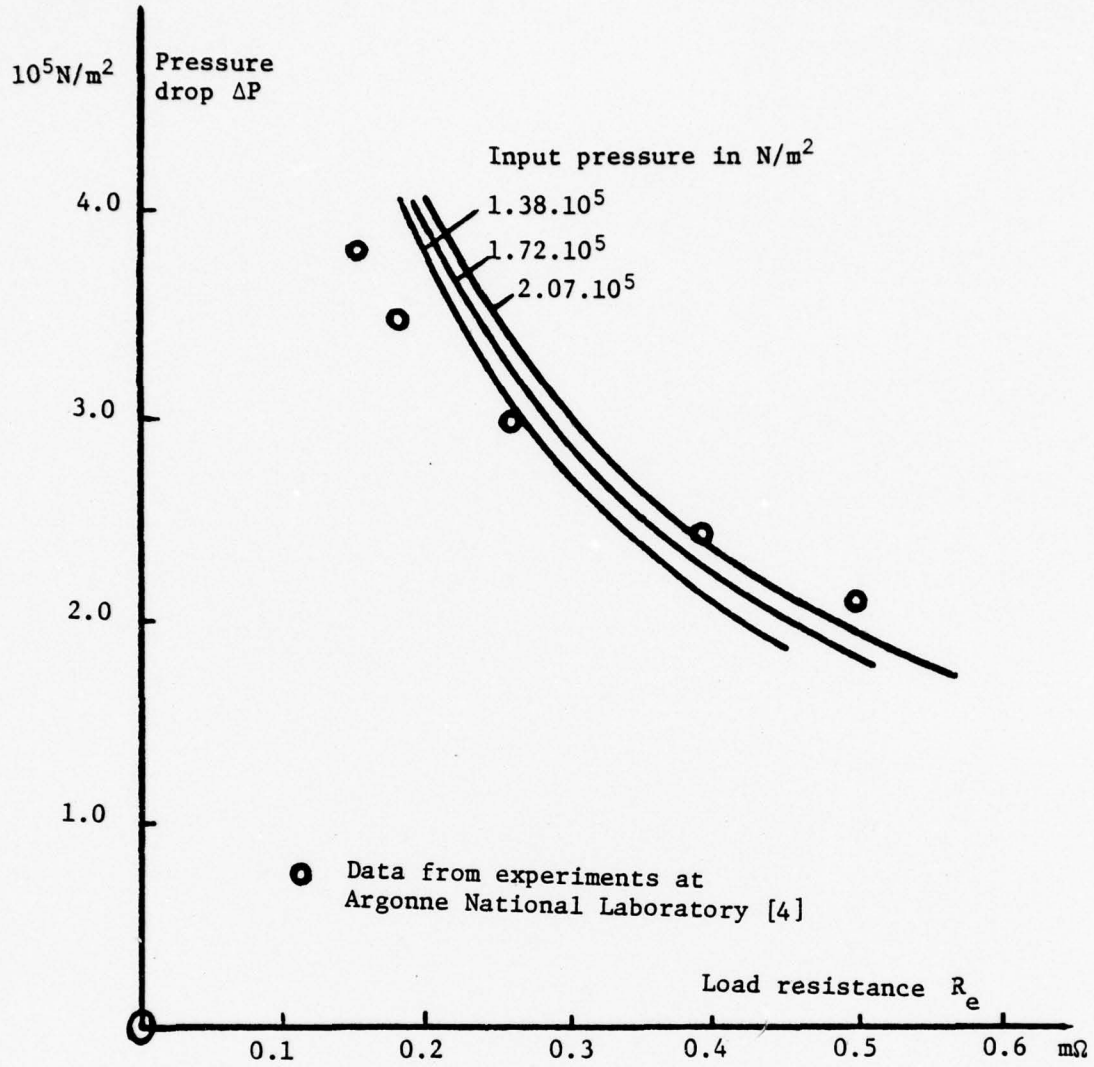

Figure 3.1: Graph of pressure drop ΔP vs. load resistance R_e for several input pressures. Curves were calculated from equation (3.11) for a generator of the dimensions of Argonne National Laboratory's NaK/N_2 device. The void fraction for equation (3.11) is determined on the basis of a one dimensional, linear velocity distribution with no slip.

at the same velocity.

It is important to note that calculations of pressure drop are not very sensitive to the structure of the flow. Thus, success in such calculations cannot be construed to imply success in the describing the detailed flow by a given analytic model. It also is noteworthy that, in the limits of the magnetoaerodynamic approximation, equation (3.11) is valid for any flow distribution whatsoever in the generator. The fact that it can be used to describe the pressure drop in a one dimensional or slug flow by no means implies that it is limited to such cases.

It is of fundamental concern to the slip problem whether the ponderomotive interaction can resist the motion of voids independently of inertial, viscous, or surface tension interactions. Consider the motion in a slug flow of low magnetic Reynolds number and near a flat liquid/void interface. Superimpose a small rectilinear disturbance on that interface as in Figure 3.2.

With only ponderomotive forces acting on the system, there can be no pressure gradient in region A. Equation (3.1) gives the downstream velocity there:

$$u_A = \frac{E_3}{B_2} \tag{3.12}$$

The downstream velocity in region B is

$$u_B = \frac{E_3}{B_2} - \frac{1}{\sigma B_2^2} \frac{\partial P}{\partial x_1} \tag{3.13}$$

where $\frac{\partial P}{\partial x_1}$ is the pressure gradient in region B.

The interface velocity u_C must be equal to u_A. The interface velocity u_D

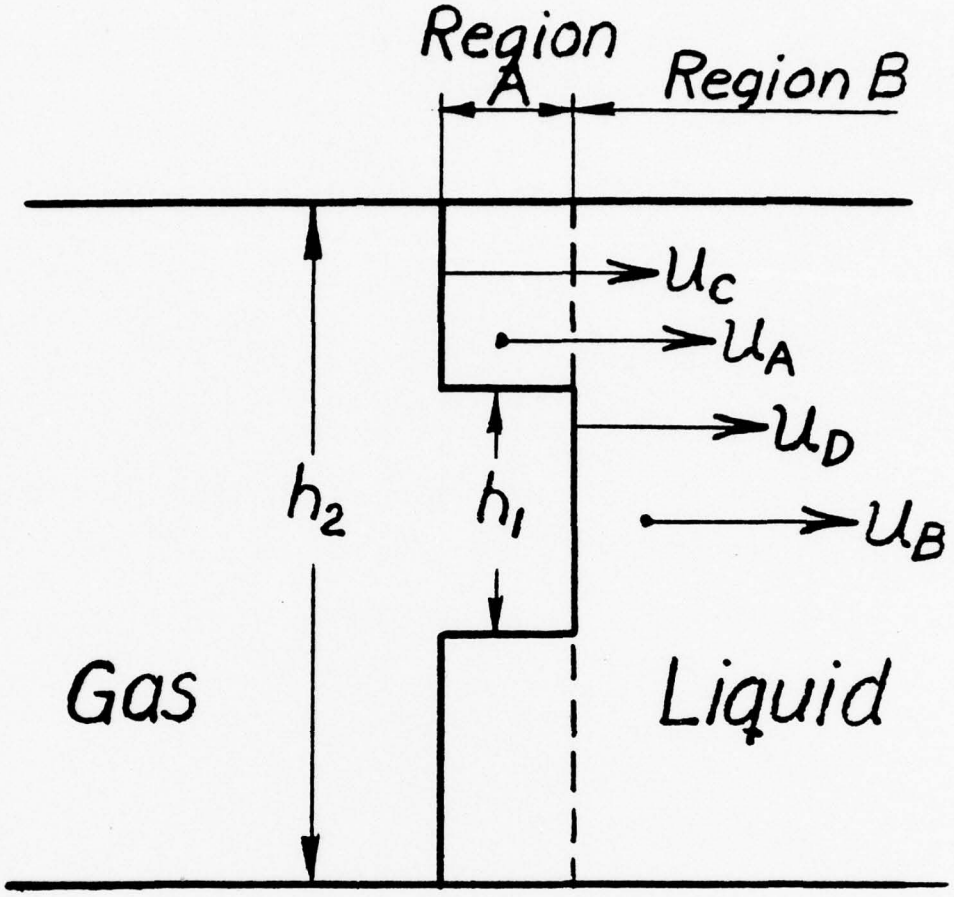

Figure 3.2 Perturbation of a gas/liquid interface.

can be found from the continuity condition

$$(u_D - u_B)h_2 = (u_D - u_C)\ (h_2 - h_1) \tag{3.14}$$

to be

$$u_D = \frac{u_B\ h_2 - u_C(h_2 - h_1)}{h_1} \tag{3.15}$$

Substitute for u_B and u_C to get

$$u_D = \frac{1}{\sigma B_2^2}\ \frac{\partial P}{\partial x_1}\ \frac{h_2}{h_1} + \frac{E_3}{B_2} \tag{3.16}$$

Evidently, the disturbance grows at a rate relative to the rest of the interface

$$u_D - u_c = -\frac{1}{\sigma B_2^2}\ \frac{\partial P}{\partial x_1}\ \frac{h_2}{h_1} \tag{3.17}$$

Disturbances of any size will grow; smaller disturbances will grow more rapidly. Similar effects appear to be characteristic of the leading edges of all voids. We infer that ponderomotive forces have a destabilizing influence on the voids. Thus, the motion of the gas must ultimately be determined by considering also inertial, viscous and surface tension forces which stabilize the motion of the voids, permitting steady states of two-phase MHD channel flows studied experimentally at the Argonne National Laboratory. It is of importance to recognize that any analysis neglecting other than ponderomotive forces cannot be valid for anything but over-all flow conditions. Similitude considerations on bubble dynamics and the slip problem are governed by a set of parameters which must be radically different from the parameters describing some averaged or over-all two-phase motion.

CHAPTER 4

TWO-DIMENSIONAL PRESSURE DISTRIBUTION

A cross stream pressure gradient arises as a consequence of the induced magnetic field. That pressure gradient can be evaluated from the averaged force balance (see equation (2.24) and the induction equation. Break the force balance into two of its vector components:

$$0 = -\frac{\partial \bar{P}}{\partial x_1} - \bar{J}_3 \bar{B}_2 \tag{4.1}$$

$$0 = -\frac{\partial \bar{P}}{\partial x_2} + \bar{J}_3 \bar{B}_1 \tag{4.2}$$

Eliminate $\bar{J}_3$ between equations (4.1) and (4.2) to get the pressure gradient ratio ϕ

$$\Phi \equiv \frac{\frac{\partial \bar{P}}{\partial x_2}}{\frac{\partial \bar{P}}{\partial x_1}} = \frac{\bar{B}_1}{\bar{B}_2} \tag{4.3}$$

The induced flux density $\bar{B}_1$ can be found by integrating the x_3 component of Ampére's law,

$$\frac{1}{\mu_e} \frac{\partial \bar{B}_1}{\partial x_2} = -\bar{J}_3 \tag{4.4}$$

to get

$$\bar{B}_1 = -\mu_e \bar{J}_3 x_2 + \bar{B}_e \tag{4.5}$$

where $\bar{B}_e$ is a constant determined by external circuit geometry and where μ_e is the magnetic permeability. The integration is possible in this form

because $\bar{J}_3$ is constant over x_2 (see equation (3.3)). Manipulation of equations (3.3), (4.3), and (4.5) leads to

$$\Phi = \frac{\mu_e \frac{\partial \bar{P}}{\partial x_1}}{\bar{B}_2^2} x_2 + \frac{\bar{B}_e}{\bar{B}_2} \tag{4.6}$$

which demonstrates an interesting dependence of pressure gradient ratio on applied magnetic flux and downstream pressure gradient. When the x_2 origin is located at the center plane of the channel and when, as in the Argonne experiments, the external electric current is returned through two equal sheets just outside the channel, then the $\bar{B}_e$ of equation (4.6) is identically zero and the cross stream pressure gradient is maximum in magnitude at the channel walls.

The permeability of free space is equal to $4\pi.10^{-7}$ H/m. In the Nak-N_2 facility at ANL, $\frac{\partial P}{\partial x_1}$ is about 10^6 N/m^3, $\bar{B}_2$ is about one Tesla, and the channel half width is about 0.01 m. The maximum magnitude of Φ, then is

$$\Phi_{max} = \frac{4\pi.10^7 \ .10^6 \ . \ 0.01}{1} = 0.013 \tag{4.7}$$

In the proposed full scale generator, $\frac{\partial \bar{P}}{\partial x_1}$ and $\bar{B}_2$ would have about the same values, but the channel half width would be about 0.1 m., so that we would have

$$\Phi_{max} = 0.13 \tag{4.8}$$

These induced cross stream pressure gradients may well be important in phase separation, as gas voids will tend to slip along the negative pressure gradient towards the center of the channel.

CHAPTER 5

PHASE SLIP IN THE FARADAY GENERATOR

The motion of an isolated bubble entrained in a flow through a Faraday generator can be examined by a drag coefficient approach. The bouyancy force F_B on such a bubble is

$$F_B = - \frac{\partial P}{\partial \xi} V = \sigma B_2^2 \hat{u}_1 (1-K) V \qquad (5.1)$$

where $\frac{\partial P}{\partial \xi}$ is the local pressure gradient which we approximate by the downstream pressure gradient. V is the volume of the bubble, and K is the ratio of external to total electrical resistance. The resistance force F_R on the bubble we express as

$$F_R = \frac{1}{2} C_D \rho u_s^2 A \qquad (5.2)$$

where C_D is the drag coefficient for the bubble, u_s is the velocity of the bubble relative to its surrounding medium, and A is the cross sectional area of the bubble. We equate F_B and F_R and solve for u_s to find

$$u_s = \left(\frac{2V}{\rho C_D A} \left(- \frac{\partial P}{\partial \xi} \right) \right)^{1/2} = \left(\frac{2V \sigma B_2^2}{\rho C_D A} \hat{u}_1 (1-K) \right)^{1/2} \qquad (5.3)$$

For the NaK - N_2 system operating with a $\frac{\partial P}{\partial \xi}$ of 10^6 N/m^3, V/A of 0.003 m, a liquid density of 850 kg/m^3, and an assumed C_D of 2 , we find that u_s is about 1.9 m/s.

The major uncertainty in the above formula is the value of the drag coefficient as a function of the magnetic field. The theoretical results of Chester [9] are clearly not applicable to the large Hartmann number case

existing in the MHD duct flows. However, the recent experimental work of Mori et al [10] may find some application. Their results on the rise of millimeter size bubbles in a vertical column of mercury in the presence of a transverse magnetic field indicate that the bubble drag coefficient is directly proportional to the magnitude of the applied magnetic field. The effect of Reynolds number in these experiments is not clear.

If a pressure gradient induces a local slip in the flow, then a cross stream pressure gradient will induce a cross stream component of the slip. Thus, voids in the generator would "rise" down the pressure gradient towards the low pressure region at the center of the channel. This might lead to an accumulation of voids in the central regions at the expense of the wall near regions. Equation (3.1) is an expression of local liquid velocity as a function of local void fraction. As voids accumulate in the center of the channel, the liquid remaining there accelerates while the liquid collecting at the walls decelerates. This process might continue until electrical connectedness is lost in the large void fraction regions or until the model otherwise breaks down. It is possible that a substantial portion of the total portion of the total pressure energy could be transferred to kinetic energy of this high velocity material.

Geometric arguments lead to an upper bound on the maximum local slip permissible if complete phase separation is to be avoided. Consider a single void entrained in the flow within the generator. If the flow is locally isotropic, then the void will slip at a velocity u_s in the direction of the local pressure gradient relative to the void's surrounding medium. The total velocity u_T of the void is equal to the vector sum of u_s and the velocity of u_c of the surrounding medium. This is shown diagrammatically in Figure 5.1

where u_{s_1} and u_{s_2} are the resolved components of u_s. Suppose that, in the generator, the voids are distributed uniformly initially, and thereafter drift monotonically towards the center of the channel at a velocity dependent only on cross stream pressure gradient. The two phases will be separated completely by the time a void beginning near a wall has drifted a one $\hat{\alpha}$: th part of the distance to the center of the channel. Once this has occurred, the channel can no longer act as an effective generator. Thus, for any given channel and set of operating conditions, there is a maximum permissible local slip if generator effectiveness is not to be lost through phase separation. From Figure (5.1) we infer that if the channel has a length ℓ and a width 2a, then

$$\frac{u_c + u_{s_1}}{u_{s_2}} \geq \frac{\ell}{\hat{\alpha}\, a} \tag{5.1}$$

if the phases are not to be completely separated. Additionally, if the void is to slip in the direction of the local pressure gradient relative to the surrounding medium, then

$$\frac{u_{s_2}}{u_{s_1}} = \frac{\frac{\partial \bar{P}}{\partial x_2}}{\frac{\partial \bar{P}}{\partial x_1}} = \Phi \tag{5.2}$$

Finally, we have approximately for $u_c >> u_{s_2}$ that

$$u_c + u_{s_1} = k u_c \tag{5.3}$$

where k is the local slip ratio.

The slip velocities can be eliminated between equations (5.1), (5.2), and (5.3) to give

$$k \leq \frac{1}{1 - \frac{\hat{\alpha}\, a}{\ell} \cdot \frac{1}{\Phi}} \tag{5.4}$$

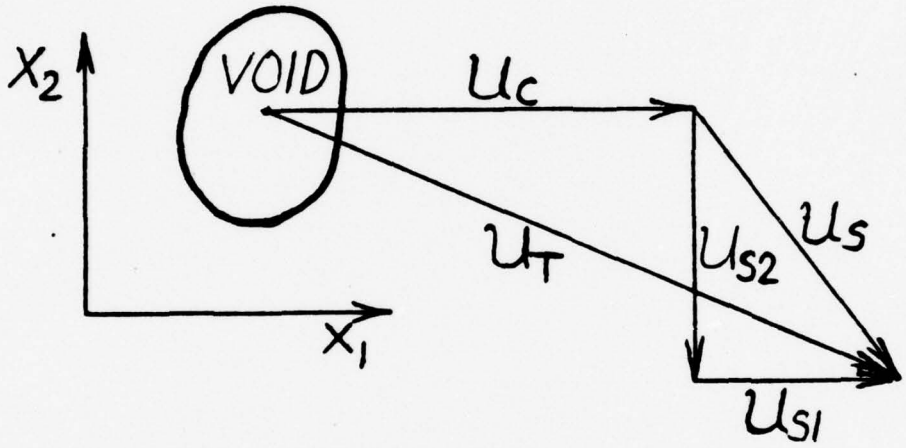

Figure 5.1. Definition of slip of a void in cross stream and upstream pressure gradient.

For the NaK-N_2 facility at Argonne National Laboratory , with $\frac{\hat{\alpha}\, a}{\ell}$ about 0.125, $\hat{\alpha}$ about 0.5, and Φ about 0.013, we find that $k \leq 2$. In the full scale generator as projected in reference [2], with $\frac{\hat{\alpha}\, a}{\ell}$ about 0.125, $\hat{\alpha}$ about 0.5, and Φ about 0.13, we find that $k \leq 1.05$. This letter figure represents a smaller slip than one might reasonably expect for a bubbly flow. Hence, one might expect large void fraction gradients to develop in the full scale generator.

CHAPTER 6

FINITE DIFFERENCE CALCULATIONS FOR TWO-DIMENSIONAL HARTMANN FLOWS WITH CROSS-STREAM DEPENDENT ELECTRICAL CONDUCTIVITY

The finite difference calculations reported on in our previous annual report [1], have been extended to higher Hartmann numbers and to a variety of electrical conductivity profiles. We have retained our simplifying approximation that the two-phase flow in an MHD generator duct of rectangular cross-section be replaced by a homogeneous flow with cross-stream dependent electrical conductivity and constant viscosity. This is motivated by the fact that viscous effects are important only in regions very near the walls. Those regions are thin enough that, over them, the viscosity is essentially constant. Determination of the velocity and electric current fields reduces from eqs.(2.14) and (2.15) to solution of the two coupled partial differential equations

$$-\frac{\partial P}{\partial x_1} + \frac{1}{\mu_e} B_2 \frac{\partial B_1}{\partial x_2} + \mu\left(\frac{\partial^2 u_1}{\partial x_2^2} + \frac{\partial^2 u_1}{\partial x_3^2}\right) = 0 \qquad (6.1)$$

$$\mu_e B_2 \frac{\partial u_1}{\partial x_2} + \frac{\partial}{\partial x_2}\left(\frac{1}{\sigma}\frac{\partial B_1}{\partial x_2}\right) + \frac{\partial}{\partial x_3}\left(\frac{1}{\sigma}\frac{\partial B_1}{\partial x_3}\right) = 0 \qquad (6.2)$$

where the conductivity σ is a function of x_2 and x_3. This set of equations is solved subject to the MHD generator boundary conditions that the velocity u_1 vanishes at the insulating walls, $x_2 = \pm a$, and at the electrodes, $x_3 = \pm b$. In addition, B_1 is constant along the insulating walls, and the tangential component of the electric field vector as well as the normal component of the magnetic field vector is continuous at the electrode surfaces, $x_3 = \pm b$. We have carried out finite difference solutions of eqs. (6.1) and (6.2) using the Peaceman-Rachford alternate direction implicit method (see Michell [11])

for specified symmetric conductivity distributions with respect to the channel axis and for given values of the channel aspect ratio $\lambda = 2b/2a$, non-dimensional electrode conductivity K_w load factor K; and Hartmann number $M = aB_o\sqrt{\sigma_o/\mu_o}$, where the o subscripts indicate properties of the pure liquid, i.e. in the immediate vicinity of the channel walls. (K_w is the ratio of resistance of electrodes plus fluid; and again K is the ratio of external to total electrical resistance.)

In order to secure rapid convergence, it was found neccesary to use a variable grid spacing such that there are approximately as many points located within the thin Hartmann layer of thickness a/M along the insulating walls and the electrode boundary layer of thickness $a\sqrt{M}$ along the conducting walls along the conducting walls of the channel as there are points in the core. Because of the assumed symmetry in viscosity and electrical conductivity with respect to the channel axis, it is sufficient to carry out the calculations over only the first quadrant of the channel cross-section $0<x_2<a, 0<x_3<b$. We typically found solution convergence at M = 100 after one hundred iterations when using a 1200 grid point subdivision of the channel quadrant. The convergence was much more rapid at lower Hartmann numbers, while calculations at higher M generally required a larger number of grid points and hence larger CPU times for convergence.

Typical results of the finite difference calculations are shown in Figures 6.1 through 6.5. Figure 6.1 presents the velocity contours for Hartmann flow of a constant conductivity fluid in a channel of aspect ratio $\lambda = 2a/2b = 2$. The Hartmann number is M=100, the load factor K = 0.91 with ideally conducting electrodes. Note the very thin Hartmann layers near $x_2=\pm a$ of thickness a/M and the thicker electrode boundary layers at the conduct-

ing walls having thickness of order $a/\sqrt{M}$. The constant velocity core away from the walls represents that portion of the channel cross-section where the pressure gradient just balances the Lorentz force and where viscous effects are unimportant. The corresponding curves of constant induced magnetic intensity and hence the current streamlines within the channel are shown in Figure 6.2. Note that except in the wall near boundary layer regions the current is uniform. Apart from channel end conditions and streamwise flow variations, shunt currents occur only in the thin viscous layers along the insulating walls and become negligible as the Hartmann number becomes large, provided the external load resistance remains finite. For infinite external loads all the current generated within the core of the flow would be returned through the Hartmann layers.

The effect of a cross-stream variation in electrical conductivity on two-dimensional Hartmann flow at M= 100 is shown for a channel of aspect ratio $\lambda = \frac{1}{2}$ in Figures 6.3 through 6.5. Because of the flow cross-section symmetry, we are showing only one quadrant of the channel section in these figures. The conductivity used in these calculations has the parabolic distribution

$$\sigma = \sigma_o \{1-c\ [1-(x_2/a)^2][1-(x_3/b)^2]\}\ , \qquad (6.3)$$

where σ_o is the pure liquid conductivity and c is an adjustable constant ranging from zero for the constant conductivity case to a value of unity corresponding to a variable conductivity flow with zero electrical conductivity along the channel axis. This particular parabolic variation of the conductivity approximately simulates the void fraction distribution observed in the experiments at Argonne National Laboratory [2]. Note that the low conductivity core region develops a high velocity jet, the velocity being an

approximate reciprocal function of the electrical conductivity. This is in contrast to the flat velocity profile obtained for the case of constant conductivity.

In addition to the above finite difference calculations,we have also obtained values for the volume flow rates and generator conversion efficiency as a function of pressure gradient, Hartmann number, load factor, electrode conductivity, channel aspect ratio and cross-stream conductivity variation. Among other things, these additional results show that for infinite external load the maximum flow rate at constant conductivity occurs through channels of aspect ratio less than unity,supporting results reported by Hughes and Young [6]. For example at M= 10 the maximum flow rate occurs near $\lambda = 0.3$ compared to $\lambda = 1.0$ in the non-magnetic case. We attribute this effect to larger drag being produced by the viscous layers along the insulating walls than by the thicker viscous layers along the electrode surfaces. We will report more about these findings in the next chapter.

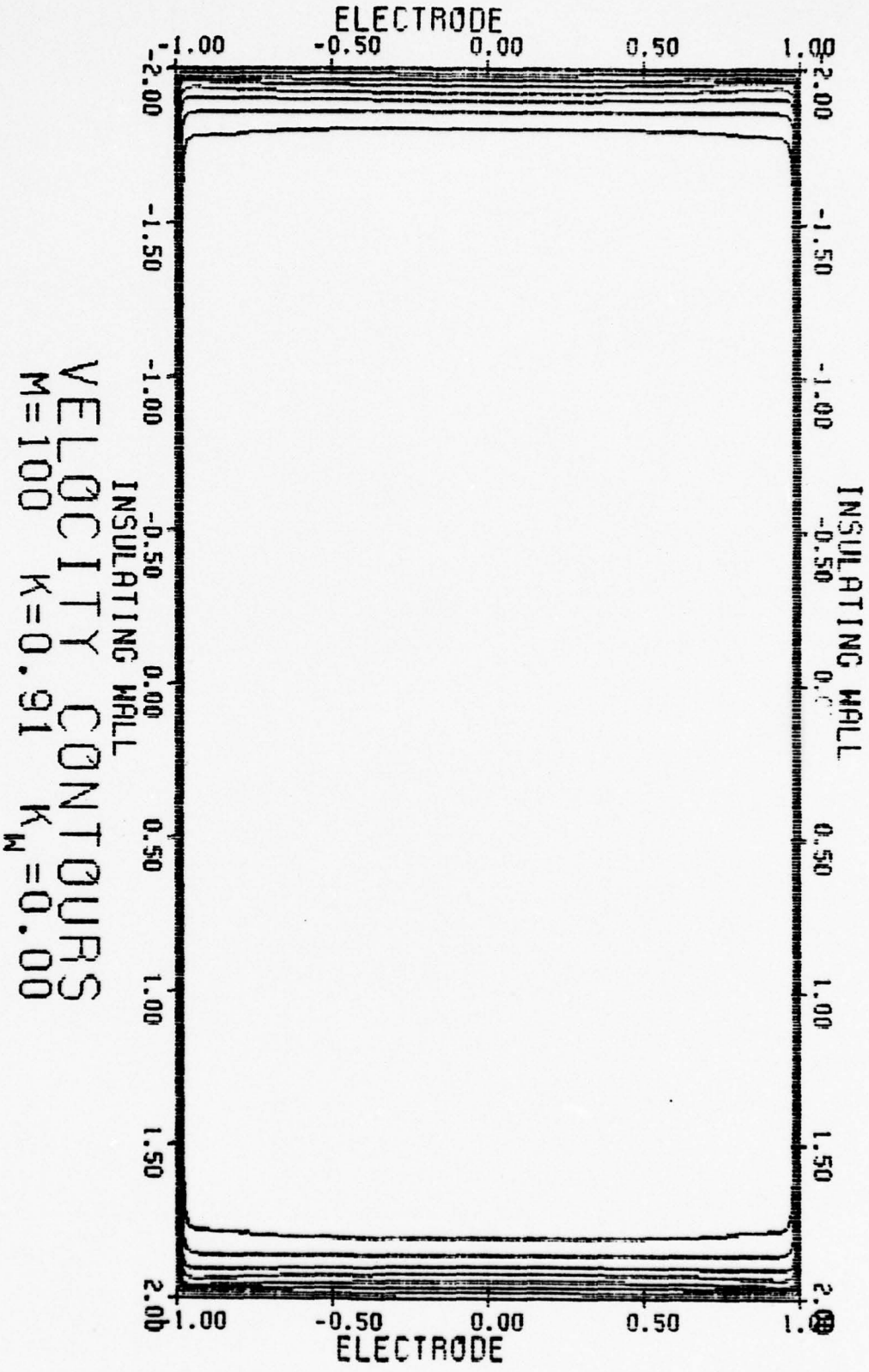

Figure 6.1 Velocity contours for two-dimensional Hartmann flow. The fluid has uniform electrical conductivity. Hartmann number M=100. Load factor K=0.91. Channel aspect ratio λ=2. The electrodes are ideal conductors.

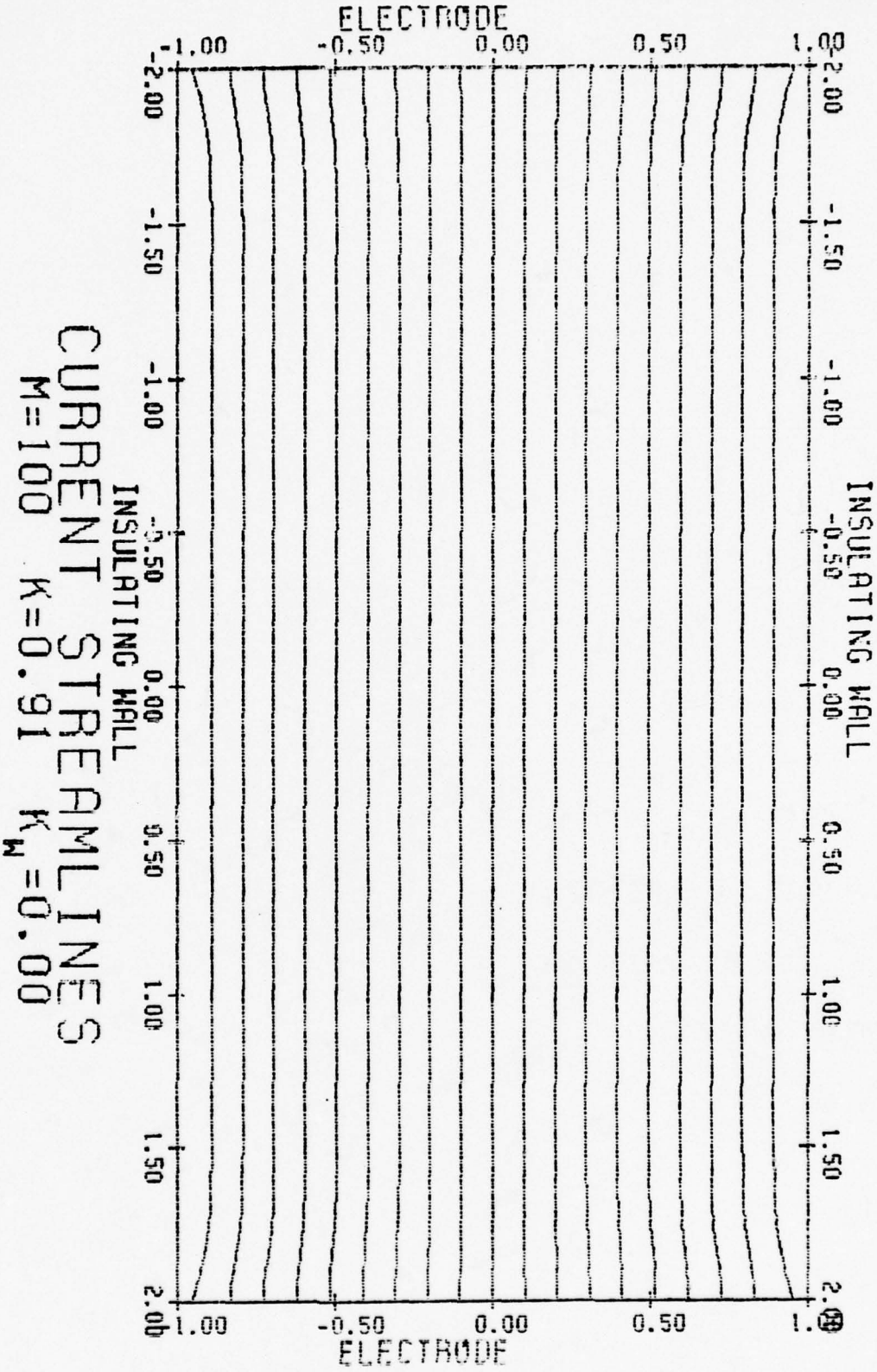

Figure 6.2 Current streamlines for two-dimensional Hartmann flow under conditions identical with those given in Figure 6.1.

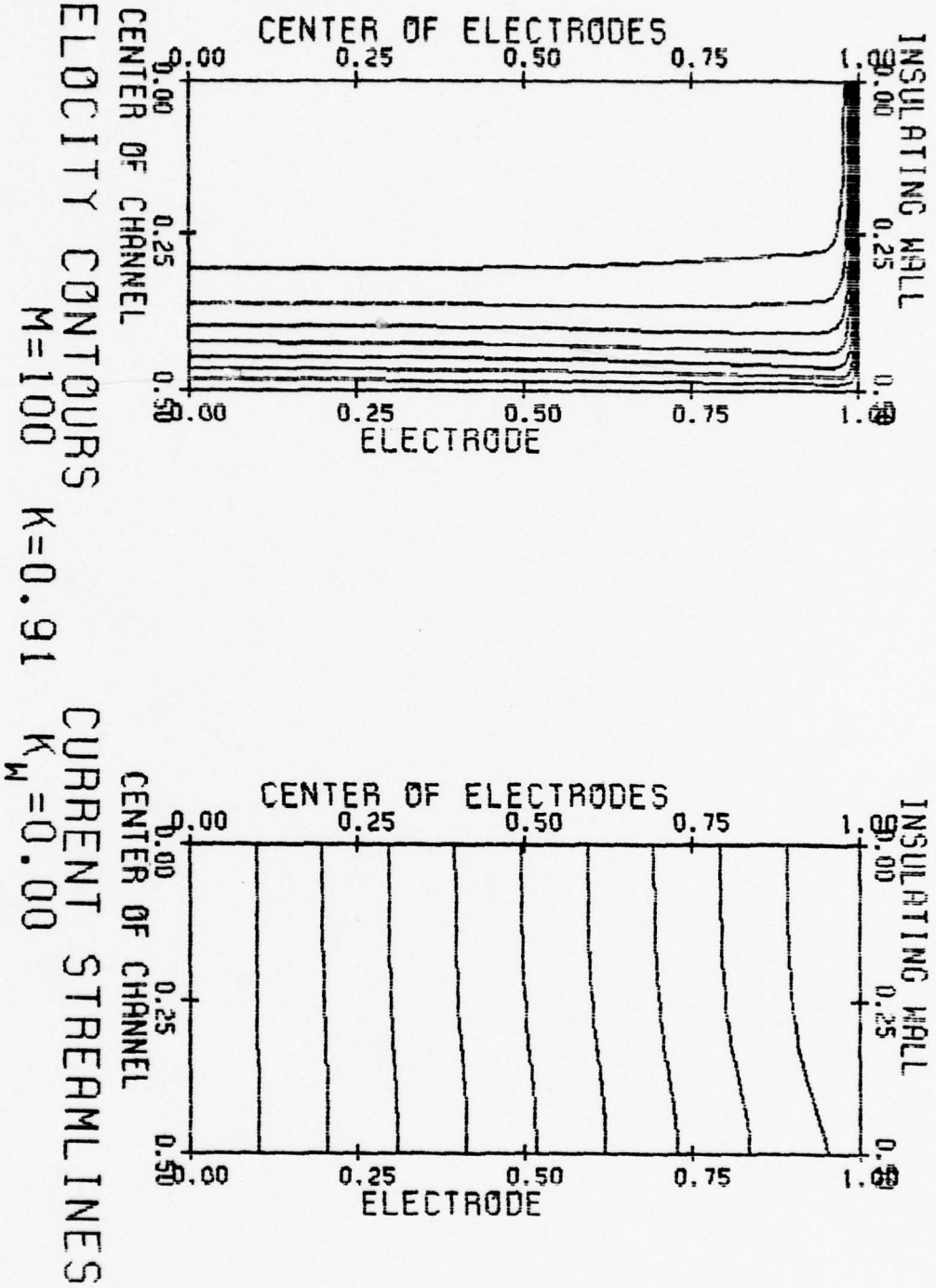

Figure 6.3 Velocity and current contours over a λ=0.5 aspect ratio channel cross-section. Hartmann number M=100. Uniform electric conductivity of the fluid.

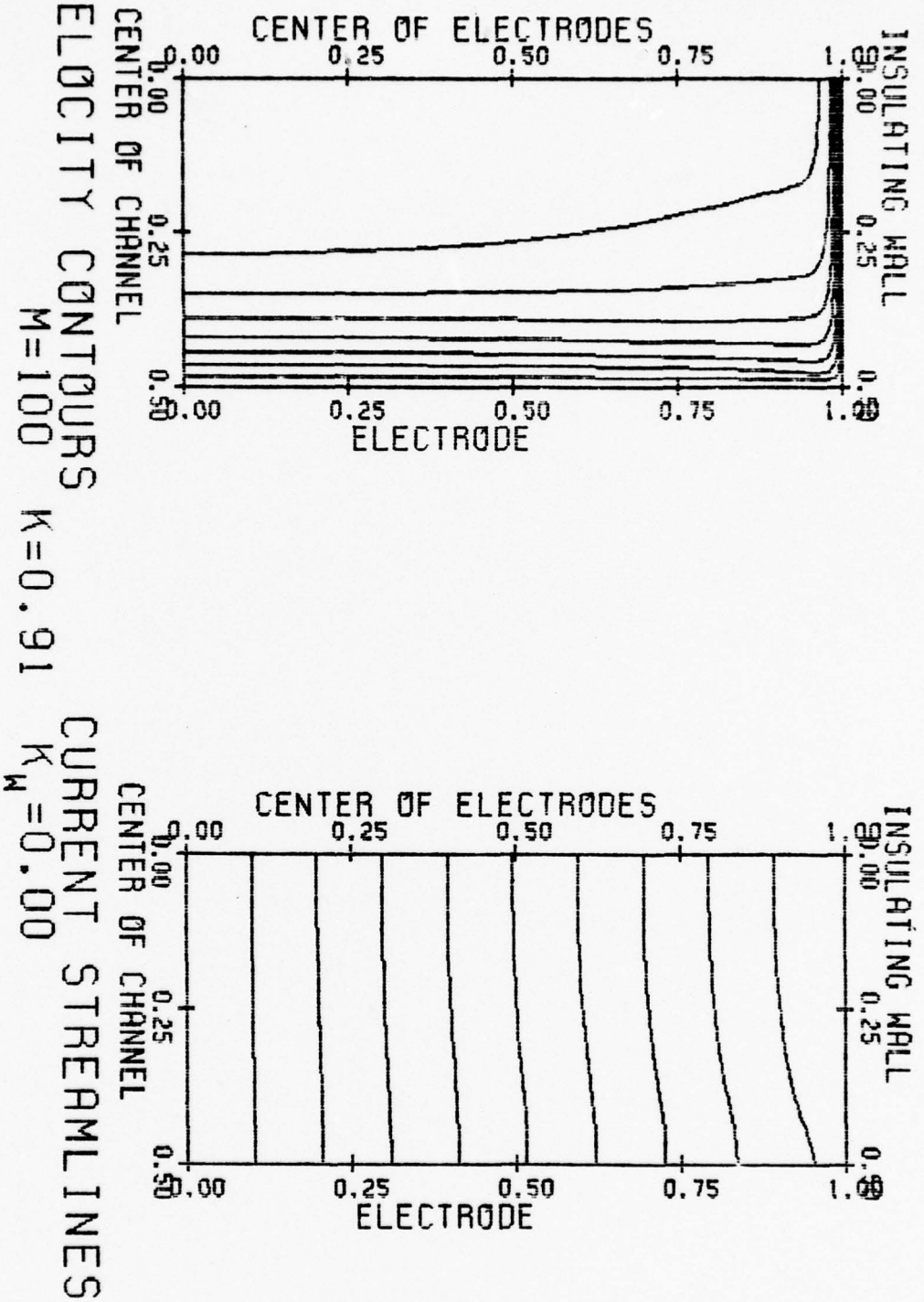

Figure 6.4 Velocity and current contours for M=100, λ=0.5 and K=0.91. Conductivity distribution according to eqin (6.3), c=0.5.

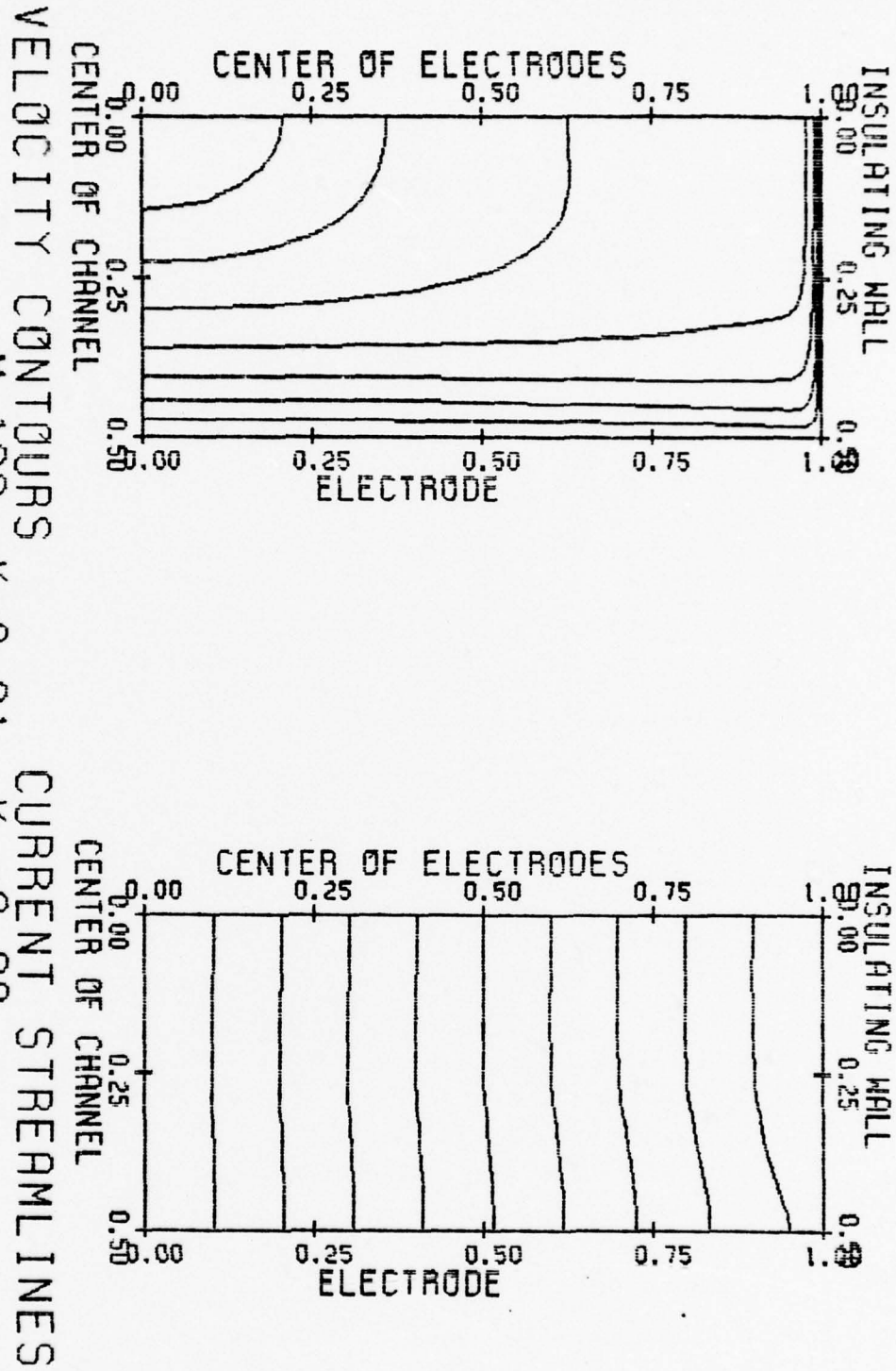

Figure 6.5 Velocity and current contours for M=100, λ=0.5 and K=0.91. Conductivity distribution according to eq:n (6.3), c=0.9. Note the Inflected Velocity Profile.

CHAPTER 7

ANALYTICAL APPROXIMATION

In view of the very thin boundary layers found in our numerical calculations, it is clear that viscous effects are confined primarily to the wall near regions of the MHD duct and that the flow core comprises an essentially inviscid flow in which the Lorentz force is balanced by the pressure gradient. This suggests that an appropriate boundary layer approximation ought to be applicable to this problem in the sense that an inviscid core solution can be matched to a wall near viscous solution. In the wall near region we have approximated the boundary layer profile by

$$u_{1BL}(x_2, x_3) = \text{const.} \left(1 - \exp M \frac{x_2 - a}{a}\right)\left(1 - \exp \sqrt{M} \frac{x_3 - b}{a}\right) \tag{7.1}$$

where $M = aB\sqrt{\sigma_o/\mu_o}$ is the Hartmann number based on the half channel height a. Motivation for this choice is the known thickness of the Hartmann and electrode boundary layers. The constant multiplying this velocity distribution is adjusted so as to match the inviscid core velocity (see equation (2.24)

$$u_{1 \text{ core}} = \frac{1}{\sigma B_2^2}\left(-\frac{\partial P}{\partial x_1} - \frac{E_3}{B_2}\right) \tag{7.2}$$

where σ is the electrical conductivity which may vary over the cross section. By making the approximation that the electric field is uniform in the channel (see Chapter 3) we can use Ohm's law to eliminate E_3 from equation (7.2) and find the velocity profile

$$u_1(x_2,x_3) = -\frac{1}{\sigma_o B_2^2}\frac{\partial P}{\partial x_1}\left(\frac{1}{\sigma/\sigma_o} + \frac{1 - \frac{1}{M}}{\left[1 - \frac{1}{\lambda\sqrt{M}}\right]\frac{R_i}{R_e} + \frac{1}{M}}\right) \cdot \left[1-\exp \frac{M}{a}(x_2-a)\right]\left[1-\exp \frac{\sqrt{M}}{a}(x_3-b)\right] \tag{7.3}$$

From this result it is straightforward to determine the average velocity $\hat{u}_1$, and the corresponding electric field existing in the channel.

We have evaluated equation (7.3) for several different conductivity distributions including constant conductivity $\sigma = \sigma_o$ and the parabolic distribution given by eq:n (6.3). For a constant conductivity flow we find, for example, that the ratio of the average fluid velocity in units of $-\frac{\partial P}{\partial x_1} / \sigma_o B_2^2$ is predicted by our analytical boundary layer approximation to be 14.96 for a channel of aspect ratio $\lambda = 1$, M= 100 and resistance ratio $R_e/R_i = 17.1$. This compares to a value of 14.99 obtained with our twelve hundred variable grid point finite difference numerical calculation under identical flow conditions. For the variable parabolic conductivity, with $c = \frac{1}{2}$, we find that the non-dimensional velocity along the channel axis for M= 100, a= 1, λ= 2 and $R_e/R_i = 10$ is 11.43 by the boundary layer theory compared to 11.40 by the finite difference method. These results, together with other cases, are found to be fairly close to those obtained by the numerical method provided that $\lambda\sqrt{M}>8$ and the conductivity does not vanish. This shows that equation (7.3) is a good approximation to the true two-dimensional Hartmann profile for fluids with cross-stream dependent electrical conductivity. We also observe directly from equation (7.3) that the core velocity profile is not flat when the electrical conductivity varies in the cross-stream direction. We typically have a high velocity jet structure near the axis of the channel when the conductivity decreases toward the channel axis.

From the boundary layer approximation we find that the ratio of the volume flow rate Q to Q_{slug} obtained when neglecting the thickness of the boundary layers for the case of infinite external load, is

$$Q/Q_{slug} = 1 - \frac{1}{\lambda\sqrt{M}} - \frac{1}{M} + \frac{1}{\lambda M\sqrt{M}} \qquad (7.4)$$

and yields 0.55, 0.89 and 0.97 at M= 10, 100 and 1000, respectively, when $\lambda = 1$. This approximation is in quite good agreement with that given by Shercliff [12]

$$Q/Q_{slug} = 1 - \frac{0.852}{\lambda\sqrt{M}} - \frac{1}{M} \tag{7.5}$$

for an MHD channel flow with insulating walls all around.

The boundary layer approximation also allows the determination of the generator efficiency η as a function of resistance ratio at fixed Hartmann number and channel aspect ratio $\lambda = 2a/2b$. Defining this efficiency by

$$\eta = \frac{I^2 R_e}{-4 \frac{\partial P}{\partial x_1} ab\ell\hat{u}_1} \tag{7.6}$$

where I is the current in the external circuit, ℓ the channel length, $4ab\ell$ the channel volume, and $\hat{u}_1$ the mean velocity, we find

$$\eta = \frac{\frac{R_i}{R_e}\left[\left(1 - \frac{1}{M}\right)\left(1 - \frac{1}{\lambda\sqrt{M}}\right)\right]^2}{\left[\left(1 - \frac{1}{\lambda\sqrt{M}}\right)\frac{R_i}{R_e} + \frac{1}{M}\right]\left\{\left(1 - \frac{1}{M}\right)\left(1 - \frac{1}{\lambda\sqrt{M}} - \frac{1}{M}\right) + \left[\left(1 - \frac{1}{\lambda\sqrt{M}}\right)\frac{R_i}{R_e} + \frac{1}{M}\right]\left[\frac{1}{ab}\int_0^a dx_3 \int_0^b dx_2 \left(\frac{f}{\sigma/\sigma_o}\right)\right]\right\}} \tag{7.7}$$

where $f(x_2, x_3) = \left(1 - \exp M\frac{x_2 - a}{a}\right)\left(1 - \exp \sqrt{M}\frac{x_3 - b}{a}\right)$ is the boundary layer deficit and σ/σ_o is given by eq:n (6.3). A plot of this efficiency is given in Figure 7.1 for the special case of a constant conductivity flow. We note that the generator efficiency reaches a maximum at a resistance ratio R_i/R_e approximately equal to $1/\sqrt{M}$ and becomes increasingly efficient as the Hartmann number is increased. The optimum efficiency for a Hartmann number of 400, corresponding to experimental conditions by Petrick et al [2], occurs at an external resistance approximately twenty times the internal resistance.

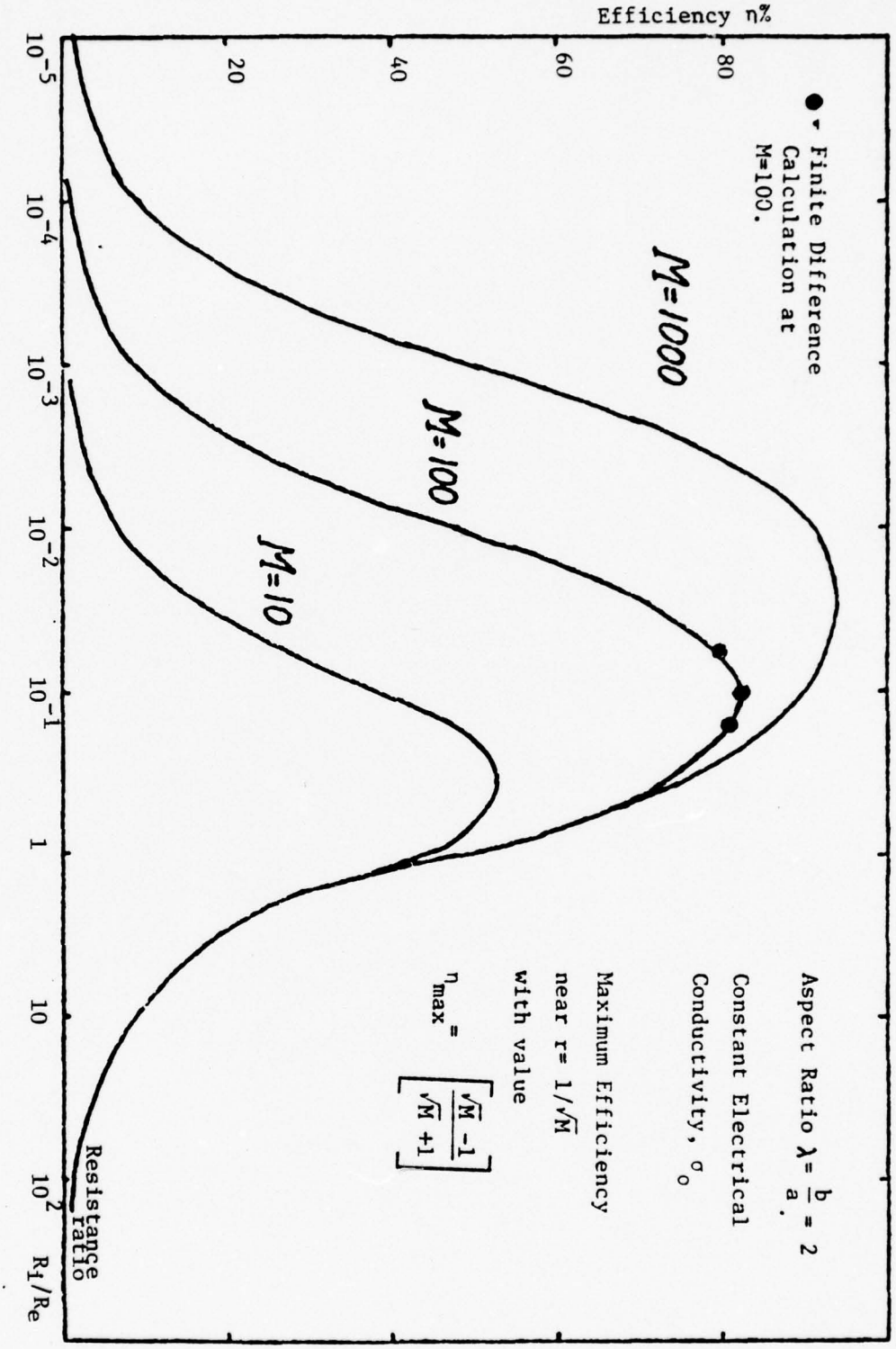

Figure 7.1 Generator efficiency as a function of resistance ratio and Hartmann number ($\lambda\sqrt{M}>>1$).

CHAPTER 8

VOLUME FLOW RATES THROUGH SUBPARTITIONED MHD CHANNELS

One of the features of the proposed two-phase MHD generator system is the tendency of the gaseous phase to slip towards the core of the generator duct. Such a cross-stream bubble drift and the experimentally observed axial slip of the gas component might be reduced by subpartitioning the MHD channel into a series of rectangular cross-section subchannels by conducting plates placed parallel to the channel electrodes and insulating plates placed parallel to the insulating sidewalls of channel. We have performed both numerical and analytical boundary layer calculations on such a subpartioned channel geometry. Velocity fields, flow rates and current stream lines have been determined. The calculations so far have been restricted to a homogeneous fluid of constant electrical conductivity.

Typical results obtained from finite difference calculations for a subpartitioned channel geometry when the subdivision consists of eight identical subchannels is shown in Figures 8.1 and 8.2. In the first of these figures we see the velocity contours corresponding to a Hartmann number of M=50 based on the half height of a subchannel and a load factor of K= 0.91. We find that the flow rate through this channel is approximately 89% of that found at the same pressure gradient when the partitions are removed. This is a relatively small reduction in flow rate produced by the partitions at the high Hartmann number under consideration. Also it is found that the largest flow rates for a given pressure gradient and infinite external load occur for channels of rectangular cross-section where the distance between the insulating walls is large relative to the distance between the electrodes. The origin for this behavior is the presence of the relatively thin Hartmann

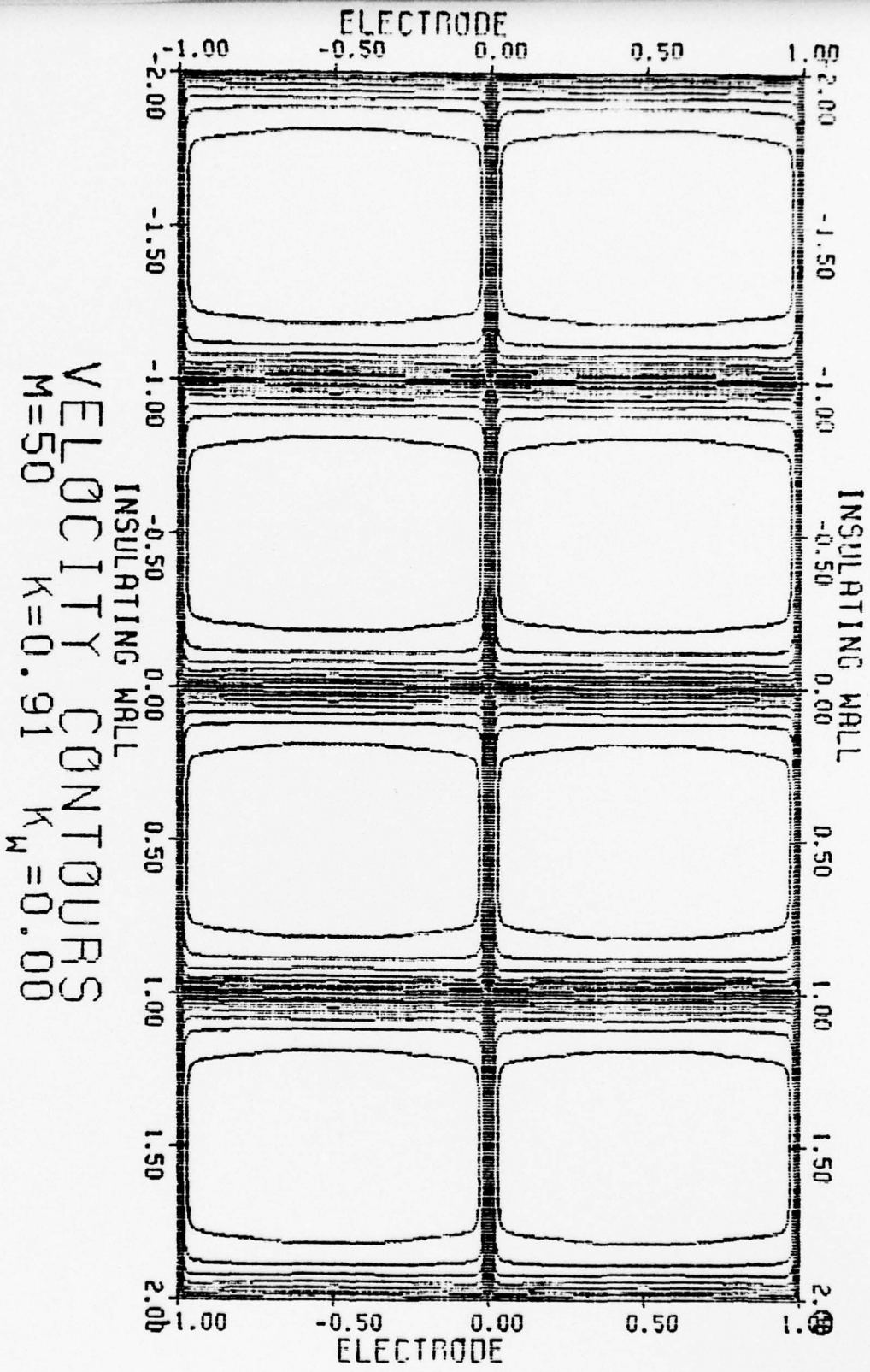

Figure 8.1 Velocity contours for an eight subchannel generator duct. Load factor, K=0.91. Hartmann number, M=50. Flow rate with partitions/flow rate in absence of partitions, 0.891.

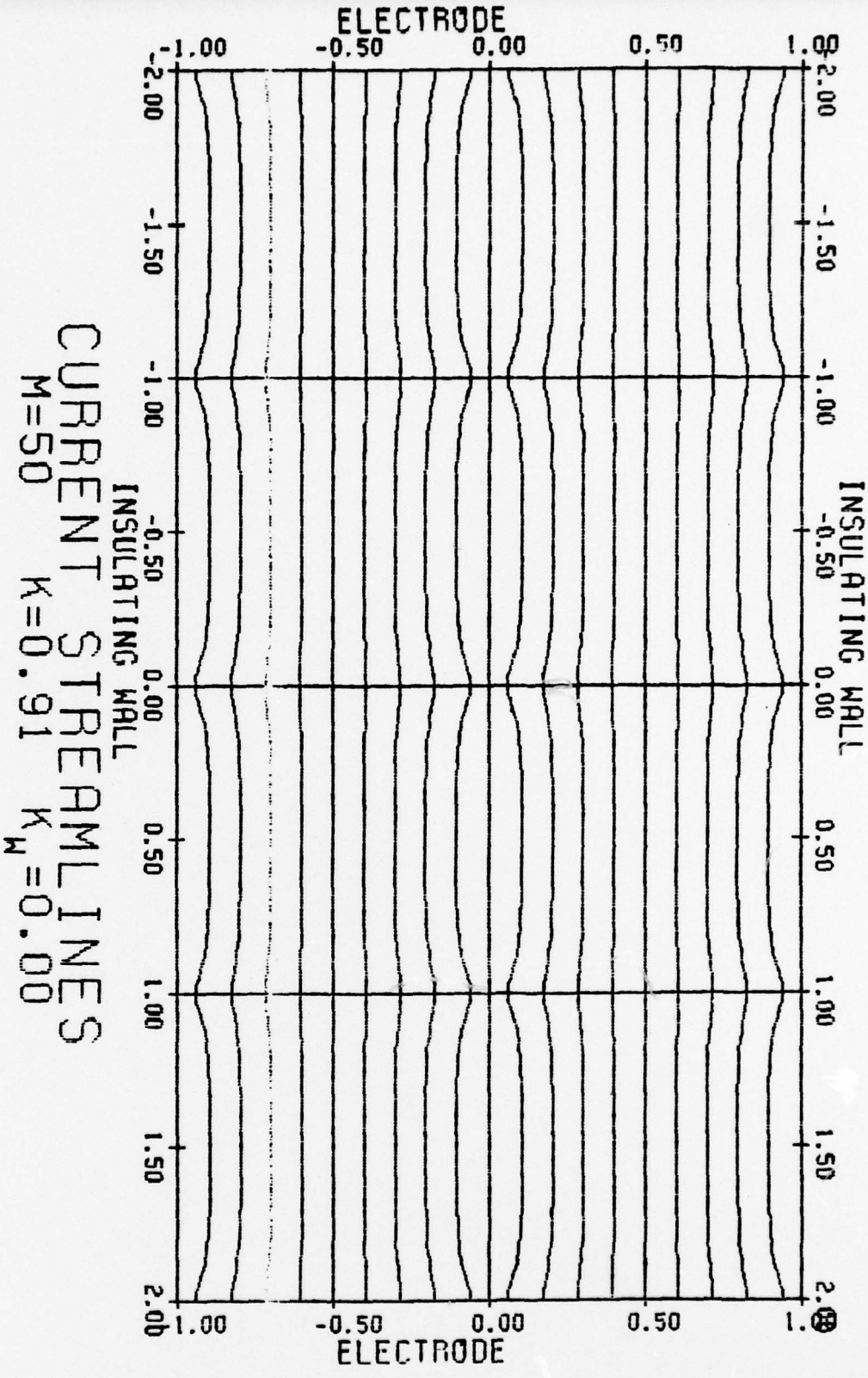

Figure 8.2 Current streamlines in a subpartitioned channel. Partitions parallel to the electrodes are perfect electrical conductors; those parallel to the insulating walls are insulators. Note the nearly uniform current density.

layer along the insulating walls compared to the thicker electrode boundary layers. We note in Figure 8.2 that the current streamlines remain nearly uniform across the subpartitioned channel cross-section. Only in the immediate vicinity of the ideally conducting subpartitions does one notice departure from uniformity.

If there are n-1 equally spaced, perfectly conducting partitions placed between the electrodes, and m-1 equally spaced insulating partitions placed parallel to the insulating walls and the aspect ratio of each of the resultant n x m subchannels denoted by $\lambda = 2b/2a$, we find that the ratio of the volume flow rate with the partitions to the volume flow rate without partitions is

$$r = \frac{\left(1 - \frac{1}{\lambda\sqrt{M}} - \frac{1}{M}\right)}{\left(1 - \frac{\sqrt{m}}{\lambda n\sqrt{M}} - \frac{1}{mM}\right)} \cdot \frac{\left(1 + \frac{1 - \frac{1}{M}}{\frac{R_i}{R_e}\left(1 - \frac{1}{\lambda\sqrt{M}}\right) + \frac{1}{M}}\right)}{\left(1 + \frac{1 - \frac{1}{mM}}{\frac{R_i}{R_e}\left(1 - \frac{\sqrt{m}}{\lambda n\sqrt{M}}\right) + \frac{1}{mM}}\right)} \qquad (8.1)$$

Again, M is the Hartmann number based on the channel half height and $R_i = bn/am\sigma_o\ell$ the internal resistance. It should be noted that this approximation holds only as long as M is large enough ($\lambda\sqrt{M}>8$). For sixteen subchannels with n=m=4, aspect ratio $\lambda=2$, resistance ratio $R_e/R_i = 10$ and a Hartmann number of M= 100 based on the subchannel half height, the above formula predicts a flow rate ratio of 0.922, supporting our notion that the viscous losses produced by a moderate number of subpartitions may be small for large Hartmann number flows.

Our overall conclusion is that use of subpartitioned channels to reduce both cross stream bubble drifts and also possibly axial bubble slip may offer

a possibility for improving the efficiency of two-phase liquid metal-MHD generators.

CHAPTER 9

SIMILITUDE IN THE TWO-PHASE FARADAY GENERATOR

Evidently, two principles govern motion of the fluids in a two-phase Faraday generator. Except very close to the physical boundaries, the ponderomotive forces alone are sufficient to account for much of the behavior of the liquid phase once its physical distribution is known. The gas phase, on the other hand, moves in the pressure gradient induced by the liquid motion, but under the influence of inertia, viscosity and surface tension. The void motion seems to do relatively little to change the local ponderomotive pressure gradient.

These considerations imply that two velocity scales exist in the two phase generator. The one scale, velocity U_L of the liquid relative to the test frame, is important in determining the ponderomotive force on the liquid. The other scale, velocity U_{LG} of the gas phase relative to the liquid phase, is important in determining the gas/liquid interaction. There is not necessarily any direct relationship between these two scales. Similitude experiments should model each separately.

Any means of creating a pressure gradient in a liquid without directly influencing a gas phase should allow modeling of the gas/liquid interaction in a two phase generator. A vertical two phase flow can be used in this fashion to model the ponderomotive pressure gradient with a gravity induced pressure gradient. The gas/liquid interaction in such an experiment should be completely specified by the geometry of the system and by the pressure gradient $\frac{\partial P}{\partial x}(=(1-\alpha)\rho g$ in the gravity model), length scale L, relative velocity scale U_{LG}, mass density ρ, viscosity μ, and surface tension γ. There are many ways in which these para-

meters can give three dimensionsless groups characterizing the flow. Any one member of such a set can be taken to be a function of the other two. Thus, in a similitude experimental designed to investigate phase slip, the relative velocity scale U_{LG} should appear in only one of a set of three dimensionless groups. This suggests the set, for example,

White and Beardmore property group (Wallis, [13])

$$K_F = \begin{cases} \dfrac{\frac{\partial P}{\partial x}\mu^4}{\gamma^3\rho^2} & \text{for generator} \\ \dfrac{(1-\alpha)g\mu^4}{\gamma^3\rho} & \text{for gravity model} \end{cases} \tag{9.1}$$

Suratman number (Ryley, [14])

$$Su = \frac{\gamma\rho L}{\mu^2} \tag{9.2}$$

drag coefficient

$$C_D = \begin{cases} \dfrac{\frac{\partial P}{\partial x}L}{\rho U_{LG}^2} & \text{for generator} \\ \dfrac{(1-\alpha)gL}{U_{LG}^2} & \text{for gravity model} \end{cases} \tag{9.3}$$

with

$$C_D = f(K_F, Su) \tag{9.4}$$

The choice of K_F and Su as characterizing groups is motivated by the facts that they are independent of U_{LG} and that K_F is independent of L. The choice of C_D as the velocity containing group is motivated by the notion that inertial forces should be more important than viscous or surfaces forces (see the order of magnitude analysis in Chapter 2). Other formulations of the similitude , such as with Weber number and Reynolds number, are possible, but may be

difficult to implement or interpret.

The property group K_F depends only on the pressure gradient and the physical properties of the fluids. A liquid should first be chosen such that there is K_F similarity with the generator. It happens that water can be used to model a range of interesting conditions in the Nak-N_2 generator. A water-air system run at a void fraction of 0.5, for example, attains a K_F similar to the Nak-N_2 system being run at a pressure gradient of about 2×10^5 . Other generator conditions could be simulated by, for example, adding a surfactant to the water.

Once a liquid has been selected for the simulation, Su similitude determines the length scale of the gravity model. The NaK-N_2 generator, with an overall length of 0.3 m, would be simulated by a gravity model scaled to a length of about 1.5 m if water is chosen as the modeling liquid. Once K_F and Su simularity has been achieved, an experimental run such that the void fraction matches the void fraction of the generator should then model the gas/liquid interaction in the generator.

To complete the experiment, the liquid velocity scale U_L must then be modeled. This can be done by iterating on a geometric similarity principle. The U_L for the generator is known (or can be calculated from equation (3.11). Hence, the generator velocity ratio U_{LG}/U_L can be calculated once U_{LG} has been determined from an experiment in which gas is bubbled through a still liquid. That velocity ratio then can be matched in the gravity model by adjusting U_L in the gravity model. Since this adjustment is itself apt to change the void distribution, a somewhat different value for U_{LG} will probably be obtained, calling for further adjustment of U_L. This procedure would be repeated until both void fraction and velocity ratio match in generator

and gravity model. At that point, the two-phase flows in the generator and in the gravity model should be as similar as is physically possible for such an experiment.

Other choices of dimensionless groups would entail somewhat different procedures, but the above example emphasizes the need to model the two velocity scales separately. Except in regions very close to the boundaries, the bulk motion of the liquid plays little role in the gas/liquid interaction.

It must be kept in mind, however, that gravity simulation cannot exactly describe flow in the generator. One might expect trouble in attempting to model the effects of induced ponderomotive forces and of gas compressibility.

The pressure gradient in the simulation depends on local void fraction, but not on local liquid velocity as in the generator. Thus large void fraction regions conceivably can maintain large pressure gradients in the generator, but not in the simulation. Further, the cross stream pressure gradient in the generator does not necessarily exist in the simulation. (Tipping the simulated channel from vertical might partially model this cross stream gradient.) Finally, the simulation does model the effects of forces induced in the immediate vicinity of the voids. For example, a void in the generator may expand more readily in the direction of the magnetic field than across it, as pointed out by Vliet et al [15].

The gas phase will expand as it moves down the channel, and so tend to increase the observed void fraction. This effect might be allowed for in the gravity model by pulling a partial vacuum on the system. In that fashion, one could match the gas expansion in the model to that in the generator. Sonic effects may be more difficult to model. For a given void fraction and liquid density, the speed of sound in a well dispersed bubbly flow is proportional

to the square root of pressure (see references [13,1]. Thus, the speed of sound in a high pressure generator may be several times as large as the speed of sound in a low pressure simulation. Shocks and other compressibility effects observed in the gravity model may or may not be present in the generator, depending on how closely Mach number similarity happens to be met.

CHAPTER 10

CONCLUSIONS

Time averaging of the governing equations of the liquid phase leads to a number of insights into the behavior of two-phase Faraday generators. Evidently, one can describe averaged motion of the liquid phase, given only the applied flux density, liquid physical properties, and averaged void distribution. Formally, the stress state of the gas phase is largely decoupled from the stress state of the liquid phase. With these considerations, one can come to relatively simple relationships which allow statements about generator performance.

One such statement is that a peaked void distribution must lead to a peaked liquid velocity profile, but not to an increased electrical shunting near the channel walls. Before this principle was clearly understood, experiments were performed at Argonne National Laboratory [4] in which gas was injected along the insulating walls. The purpose was to blow away from these walls the low void fraction (high effective conductivity) liquid there and so eliminate a hypothetical electrical shunt. In some experiments, efficiency increased fifty percent over that with no blowing. Since that efficiency increase could not arise from elimination of a non existant electrical shunt, we infer that it must be due to bettering the coupling between the gas and liquid phases.

It is also important to the physics of the generator that ponderomotive forces dominate liquid flow in the core. In that region, the averaged force balance equation for the liquid is purely algebraic, allowing ready derivation of relationships between pressure gradient, void fraction, electric field, and other quantities. It is interesting that some of these relationships, such

as equation (3.11), are independent of the detailed flow structure and, in fact, can be easily derived from a one dimensional, slug flow description. The converse may not be true; experimental verification of a relationship derived for a slug flow does not necessarily imply that a slug flow exists in the experiment. Further, relationships such as equation (3.11) which describe forces in the liquid phase say nothing whatsover about the behavior of the gas phase and, hence, cannot by themselves be used to verify a particular two-phase model.

In contrast to the liquid phase case, treatment of gas phase motion must include consideration of inertial, viscous, and surface forces. Experimental and analytical studies related to single bubble motion in transverse magnetic fields published in the last few years by Chester [9] and Mori et al. [10], provide only limited insight into a high void fraction flow. It appears possible to gain some understanding of the gas/liquid interaction through gravity flow modeling where a gravity supported pressure gradient simulates the ponderomotive gradient of the generator. Such a study is currently under way at the Argonne National Laboratory.

In the coming year, we plan mainly to study the gas/liquid interaction in MHD flows for an understanding of the void fraction gradient development observed in experiments with Faraday generators at ANL. We particularly plan to examine the feasibility of stabilizing the two-phase flow by means of channel subpartitioning. In addition, we wish to examine end effects in the generator. Work by Branover and others [8] demonstrates large electrical shunting in the end regions and M shaped velocity profiles in the plane perpendicular to the applied magnetic field which may degrade the generator efficiency.

REFERENCES

[1] E. R. Lindgren, U. H. Kurzweg, R. E. Elkins III, and T. A. Trovillion Two-Phase Hartmann Flows in the MHD Generator Configuration, Annual Report ONR N 00014-76-C-0410, Dept. Engin. Sciences, University of Florida (Jan. 1977).

[2] W. E. Amend, H. C. Stevens and P. V. Douzvardis; Investigation of Liquid Metal MHD Power Systems, Argonne National Laboratory, Engin. Division Report ANL/ENG - 72-06 (Dec. 1972).

[3] W. E. Amend, R. Cole, J. C. Cutting and L. C. Pittenger; Experimental Two-Phase Liquid Metal Magnetohydrodynamic Generator Program, Argonne National Laboratory, Engin. Division Report, ANL/ENG-73-02 (June 1973).

[4] M. Petrick, R. Cole, J. Cutting W. E. Amend and G. Fabris; Experimental Two-Phase Liquid-Metal Magnetohydrodynamic Generator Program, Argonne National Laboratory, Engin. Division Report, ANL/ENG-75-02 (January 1975).

[5] M. Petrick, G. Fabris, E. S. Pierson , D. A. Carl, A. K. Fischer and C. E. Johnson; Experimental Two-Phase Liquid-Metal Magnetohydrodynamic Generator Program, Argonne National Laboratory, Engin. Division Report, ANL/MHD-77-3 (Sept. 1977).

[6] W. F. Hughes and F. J. Young; The Electromagnetodynamics of Fluids, John Wiley & Sons, Inc., (1966).

[7] Lawson P. Harris; Hydromagnetic Channel Flows, Technology Press of M.I.T., (1960).

[8] H. Branover, P. Gershon, and A. Yakhot; MHD Turbulence and Two-Phase Flow, Ben Gurion University of the Negev, Beer Sheva, Israel, Dept. of Mechanical Engin. Report, ME 5-77 , 1 - 25 (April 1977).

[9] W. Chester; The Effect of a Magnetic Field on Stokes Flow in a Conducting Fluid; J. Fluid Mech., 3, 304 (1957).

[10] Y. Mori, K. Hijikata, I. Kuriyama; Experimental Study of Bubble Motion in Mercury with and without a Magnetic Field; J. Heat Trans., Trans. ASME, Sec. C, 99, 404 (1977).

[11] A. R. Michell; Computational Methods in Partial Differential Equations, John Wiley and Sons, Inc., (1976).

[12] J. A. Shercliff; Steady Motion of Conducting Fluids in Pipes under Transverse Magnetic Fields, Proc. Camb. Phil. Soc., 49, 136 (1953).

[13] G. G. Wallis; One-dimensional Two-Phase Flow, McGraw-Hill, Inc., (1969).

[14] D. J. Ryley; Review: The Thermodynamic and Mechanical Interaction of Water Globules and Steam in the Wet Steam Turbine, Int. J. Mech. Sci., 4, 447 (1962).

SECURITY CLASSIFICATION OF THIS PAGE (When Data Entered)

REPORT DOCUMENTATION PAGE

READ INSTRUCTIONS BEFORE COMPLETING FORM

1. REPORT NUMBER: Dept. of Engin. Sciences Univ.of Florida Techn.Report NR 01-001
2. GOVT ACCESSION NO.
3. RECIPIENT'S CATALOG NUMBER

4. TITLE (and Subtitle): TWO-PHASE HARTMANN FLOWS IN THE MHD GENERATOR CONFIGURATION

5. TYPE OF REPORT & PERIOD COVERED: Annual Report, Dec 76-Dec 77

7. AUTHOR(s): Rush E. Elkins, III, U. H. Kurzweg, Thomas A. Trovillion, E. Rune Lindgren

8. CONTRACT OR GRANT NUMBER(s): N000014-76-C-0410

9. PERFORMING ORGANIZATION NAME AND ADDRESS
Department of Engineering Sciences
College of Engineering, University of Florida
Gainesville, Fl. 32611

10. PROGRAM ELEMENT, PROJECT, TASK AREA & WORK UNIT NUMBERS: TASK NO. NR 099-412

11. CONTROLLING OFFICE NAME AND ADDRESS
Power Program, Material Sciences Division
Office of Naval Research, 800 N. Quincy Str.
Arlington, VA. 22217

12. REPORT DATE: Feb 78

13. NUMBER OF PAGES: 54 (59 pp.)

14. MONITORING AGENCY NAME & ADDRESS (if different from Controlling Office)

15. SECURITY CLASS. (of ...): Unclassified

15a. DECLASSIFICATION/DOWNGRADING SCHEDULE

16. DISTRIBUTION STATEMENT (of this Report)

Approved for public release; distribution unlimited

17. DISTRIBUTION STATEMENT (of the abstract entered in Block 20, if different from Report)

18. SUPPLEMENTARY NOTES

19. KEY WORDS (Continue on reverse side if necessary and identify by block number)

Magnetohydrodynamics
Two-Phase Flows
Hartmann Flows
MHD Power Generators

20. ABSTRACT (Continue on reverse side if necessary and identify by block number)

Since the mass density and viscosity of the liquid in a two-phase Faraday generator are much greater than those of the gas, consideration of the liquid phase alone should lead to a good description of force distribution in the generator. Averaging the motion over the liquid phase give us a set of equations which are similar to equations describing a steady flow of a fluid with spatially variable properties. Solutions of these equations are discussed first in the limit of negligible inertia and viscosity, and then in the limit of negligible inertia and non-zero viscosity. We discuss also the

(continued)

DD FORM 1 JAN 73 1473 EDITION OF 1 NOV 65 IS OBSOLETE S/N 0102-014-6601

Unclassified

SECURITY CLASSIFICATION OF THIS PAGE (When Data Entered)

410 049

cross stream pinch pressure gradient and its possible effects on the two-phase flow. The wall region in Faraday generators is a region of very large shear and is important in determining efficient generator operation, as is demonstrated in finite difference calculations carried out under a variety of conditions and also in an analytical boundary layer approximation which has been developed. A section has also been devoted to the possibilities of improved generator efficiency by subpartitioning the generator duct. The last section concerns similitude between two-phase generators and two-phase gravity flows. There are two velocity scales in the systems which must be scaled separately.